



A Catalogue of Forbush Decreases Recorded on the Surface of Mars from 2012 Until 2016: Comparison with Terrestrial FDs

A. Papaioannou¹ · A. Belov² · M. Abunina² · J. Guo^{3,4} · A. Anastasiadis¹ · R.F. Wimmer-Schweingruber⁴ · E. Eroshenko² · A. Melkumyan⁵ · A. Abunin² · B. Heber⁴ · K. Herbst⁴ · C.T. Steigies⁴

Received: 8 June 2018 / Accepted: 9 May 2019 / Published online: 3 June 2019
© Springer Nature B.V. 2019

Abstract Forbush decreases (FDs) in galactic cosmic rays (GCRs) have been recorded by neutron monitors (NMs) at Earth for more than 60 years. For the past five years, with the establishment of the *Radiation Assessment Detector* (RAD) onboard the *Mars Science Laboratory* (MSL) rover *Curiosity* at Mars, it is possible to continuously detect, for the first time, FDs at another planet: Mars. In this work, we have compiled a catalog of 424 FDs at Mars using RAD dose rate data, from 2012 to 2016. Furthermore, we applied, for the first time, a comparative statistical analysis of the FDs measured at Mars, by RAD, and at Earth, by NMs, for the same time span. A carefully chosen sample of FDs at Earth and at Mars, driven by the same ICME, led to a significant correlation ($cc = 0.71$) and a linear regression between the sizes of the FDs at the different observing points at the respective energies at Mars and Earth. We show that the amplitude of the FD at Mars (A_M), for an energy of $E > 150$ MeV, is higher by a factor of 1.5–2 compared to the size of the FD at Earth (A_E), for a definite rigidity of 10 GV. Finally, almost identical regressions were obtained for both Earth and Mars as concerns the dependence of the maximum hourly decrease of the CR density (DM_{in}) to the size of the FD.

Keywords Interplanetary coronal mass ejections · Forbush decreases · Neutron monitors · *Radiation Assessment Detector* (RAD)

✉ A. Papaioannou
atpapaio@astro.noa.gr

¹ Institute for Astronomy, Astrophysics, Space Applications and Remote Sensing (IAASARS), National Observatory of Athens, I. Metaxa and Vas. Pavlou St., 15236, Penteli, Greece

² Institute of Terrestrial Magnetism, Ionosphere and Radiowave Propagation by N.V. Pushkov RAS (IZMIRAN), Moscow Troitsk, Russia

³ CAS Key Laboratory of Geospace Environment, School of Earth and Space Sciences, University of Science and Technology of China, Hefei 230026, China

⁴ Christian-Albrechts-Universität zu Kiel, Leibnizstrasse 11, Kiel, 24118, Germany

⁵ Gubkin Russian State University of Oil and Gas (National Research University), Moscow, Russia

1. Introduction

Galactic cosmic rays (GCRs) are omnipresent in the interplanetary (IP) space. As a result, their recorded intensity variations reflect their modulation by large structures propagating in the IP medium, like high speed streams (HSS) from coronal holes (Iucci *et al.*, 1979; Kryakunova *et al.*, 2013) and interplanetary coronal mass ejections (ICMEs) (*e.g.* Lockwood, 1971; Cane, 2000; Belov, 2009; Richardson and Cane, 2011). In the latter case, the leading shock wave of the ICME (if any) and the following ejecta could modulate GCRs, while, in the former case, HSS may form stream interaction regions (SIRs), as well as co-rotating interaction regions (CIRs), which affect GCRs. Both may result in a reduction of the cosmic ray (CR) intensity, known as the Forbush decrease (FD), as first discovered by Forbush (1938). For the past 60 years neutron monitors (NMs) have been recording the variation of GCRs at Earth and have shown that the transient GCR intensity decreases, *i.e.* FDs, demonstrate a depression on a time scale from several hours to several days (Lockwood, 1971; Cane, 2000; Belov, 2009; Papaioannou *et al.*, 2010). FDs associated with ICMEs are known as non-recurrent, while FDs associated to CIRs as recurrent as they co-rotate with the Sun following the 27 day Carrington rotation period. This categorization is based on the sporadic or the recurrent nature of their causative interplanetary disturbance (Cane, 2000; Belov, 2009; Richardson and Cane, 2011).

Apart from ground-based NMs, several researchers have employed different datasets to study GCRs and the associated FDs: i) the anticoincidence guard data on *Interplanetary Monitoring Platform* (IMP) 8 (Cane, 2000; Richardson and Cane, 2011), ii) the anticoincidence shield (ACS) of the *International Gamma-Ray Astrophysics Laboratory* (INTEGRAL) spectrometer (SPI), (Jordan *et al.*, 2009, 2011), iii) the measurements of the *Electron Proton Helium Instrument* (EPHIN) detector onboard the *Solar and Heliospheric Observatory* and *Chandra* (Heber *et al.*, 2015) and, recently, iv) Cassini's *Magnetosphere Imaging Instrument* (MIMI)/ *Low Energy Magnetospheric Measurement System* (LEMMS) measurements (Roussos *et al.*, 2017), among others. There have also been studies that attempted to track the evolution of large interplanetary structures within the heliosphere, using all observational evidence available. Although limited by the small number of spacecraft at remote heliospheric distances, such studies have provided important insight as concerns the variability of the FD characteristics and the response of GCRs to the dynamically evolving heliosphere at different radial and spatial distances (*e.g.* McDonald, Trainor, and Webber, 1981; Van Allen and Fillius, 1992; Witasse *et al.*, 2017).

The observed properties of FDs within the heliosphere are extremely variant. This is due to: a) the complexity and the interplay of their solar sources as those propagate and interact with and within the dynamical heliosphere (Belov, 2009) and b) the differences between the observing points (Möstl *et al.*, 2015). It is noteworthy that even at a radial distance of 1 AU (*e.g.* near-Earth IP space), the properties of FDs significantly vary. Belov *et al.* (2001) analyzed the factors and the dependencies that determine the magnitude of FDs. These included the intensity of the interplanetary magnetic field (IMF) and the velocity of the solar wind. From their analysis these authors introduced an index (*e.g.* the product of the maximal solar wind velocity and the maximal IMF intensity, $V_{\max} B_{\max}$) and showed that this index had a significant correlation with the average magnitude of the FDs. Moreover, even for a subset of non-recurrent FDs that are caused by ICMEs with magnetic clouds (MCs) it was possible to identify highly variable FD time profiles caused by fast, slow, and complex ICMEs (Belov *et al.*, 2015). However, the study of FDs has been fundamental for the understanding of the heliospheric environment and the processes that take place in the IP medium. Up to now, FDs still provide crucial information from these environments (*e.g.*

Papaioannou *et al.*, 2005, 2009b; Abunina *et al.*, 2013a,b; Abunin *et al.*, 2013; Abunina *et al.*, 2015; Kryakunova *et al.*, 2015).

In this article we present a complete survey of FDs events that were identified on the surface of Mars using measurements from the *Radiation Assessment Detector* (RAD) (Hassler *et al.*, 2012), onboard the *Mars Science Laboratory's* (MSL) rover *Curiosity* (Grotzinger *et al.*, 2012), observed during the maximum and declining phases of Solar Cycle 24, from 2012 to 2016. We also perform a parallel scanning of the FDs that were recorded at Earth by neutron monitors (NMs) during the same period. We select FDs identified by MSL/RAD and by NMs within the same time period and we perform a comparative statistical and correlation analysis, at the respective energies and at each observing point. In addition, we make an effort to identify the related ICMEs of the FDs (when possible) but we do not list the related HSS (if any) or the more complex interplanetary structures, which may result from the interaction of the solar sources, leading to the recorded FDs in this stage of our study.

2. Instrumentation and Data Description

2.1. Radiation Assessment Detector (RAD)

Since its landing on the Martian surface on 6 August 2012, RAD, being an energetic particle detector, has been identifying protons, energetic ions of various elements, neutrons, and gamma rays. A detailed description of the RAD instrument can be found in Hassler *et al.* (2012) and Zeitlin *et al.* (2016). On Mars, its recordings not only include direct radiation from space (*i.e.* GCRs or solar energetic particles (SEPs)), but also secondary radiation produced by the interaction of space radiation with the Martian atmosphere and ground that results on both charged and neutral particles (Ehresmann *et al.*, 2014; Köhler *et al.*, 2014; Guo *et al.*, 2017). In addition RAD delivers dose¹ and dose equivalent rates, which have been analyzed to be concurrently modulated by the Martian atmosphere changes (both diurnally and seasonally) as well as the dynamic heliospheric conditions (Guo *et al.*, 2015). On the surface of Mars, a thermal tide controls the diurnal pressure changes that in turn gives ground to a daily oscillation of the dose rate measured by RAD (Rafkin *et al.*, 2014; Guo *et al.*, 2017). In particular, there is an anticorrelation of the total dose rate measured at RAD with respect to the pressure: when the pressure increases (during the night), the total dose rate decreases and *vice versa* (during the midday). Additionally, the variation of GCRs at Mars results from Mars seasonal variations and heliospheric structure variability due to solar activity and rotation (Hassler *et al.*, 2014; Guo *et al.*, 2015). RAD measures doses in two detectors: the silicon detector B and the plastic scintillator E. The latter has a much bigger geometric factor and, thus, has much better statistics. Hence, the dose rate from E is a very good proxy for quantifying the time variation of GCRs (Guo *et al.*, 2018).

2.2. Neutron Monitors (NMs)

Neutron monitors (NMs) are standard devices that measure cosmic rays (CRs) arriving at Earth. In particular, NMs provide the most stable long term dataset of GCRs for the past 60 years and, thus, are essential for studying GCRs and associated FDs. The Sun, occasionally, emits high-energy particles that result in a significant increase in the count rate of a NM.

¹Dose is the deposited energy by particles in certain materials *per* unit mass and it is an important measurement for understanding the radiation environment in space.

Such events are called ground level enhancements (GLEs) and occur almost once *per year* (Shea and Smart, 2012; Papaioannou *et al.*, 2014). The flux of GCRs is mainly isotropic; however, the effect of the heliospheric environment leads to its solar modulation. A prominent event that signifies the effect of solar modulation on GCRs is the FD (Cane, 2000; Belov *et al.*, 2001).

Using as many as possible NM recordings, the Pushkov Institute of Terrestrial Magnetism, Ionosphere and Radio Wave Propagation (IZMIRAN) cosmic ray group has created a database of FDs and IP disturbances (<http://spaceweather.izmiran.ru/eng/dbs.html>). This database includes the results of the global survey method (GSM) (*e.g.* density, magnitude, decrement, recovery, 3D anisotropy, gradients of the CR) obtained by the data from the worldwide network of NMs throughout the period from 1957 (when continuous network observations began) up to the present (Belov, 1987; Asipenka *et al.*, 2009; Belov *et al.*, 2018). These variations of density and anisotropy of CRs are valuable and can be used effectively to study heliospheric processes, compared to the data of any single CR detector, since the GSM allows for deriving characteristics of CRs outside the Earth's atmosphere and magnetosphere (Belov *et al.*, 2018). In addition, this database includes GOES measurements (continuously updated), the Operating Missions as a Node on the Internet (OMNI) database IP data, the list of sudden storm commencements (SSCs) from ftp://ftp.ngdc.noaa.gov/STP/SOLAR_DATA/SUDDEN_COMMENCEMENTS/, the list of solar flares reported in the solar geophysical data (<http://sgd.ngdc.noaa.gov/sgd/jsp/solarindex.jsp>), as well as all relevant IP data and geomagnetic indices (K_p , which provides the deviation of the most disturbed horizontal component of the magnetic field; Dst, which that represents the axially symmetric disturbance magnetic field at the dipole equator on the Earth's surface).

3. Compilation of the FD Catalog at Mars

3.1. FD Event Selection

3.1.1. Data Handling

First we imported the continuous RAD GCR dose rate data into a dedicated database. This covers the whole time span from 2012 to 2016. The RAD rate includes the original dose rate measurements of the MSL/RAD. It has been shown that the GCR dose rate measurements delivered by RAD exhibits a significant amount of periodic variation with a frequency of 1 sol (*i.e.* a Martian day of ≈ 24 h 40 min). This is due to the variation of the atmospheric pressure during the course of one Martian day, which leads to a clear anticorrelation between RAD measured dose rate and the surface pressure (Rafkin *et al.*, 2014; Guo *et al.*, 2018). However, the simple subtraction of the pressure effect during an FD event is not feasible, since this atmospheric effect is not constant but depends on solar modulation of GCRs (Guo *et al.*, 2017). The reliable identification of FD events in the RAD dose rate measurements requires the application of a notch filter that suppresses the effect of the diurnal variation in the data but leaves other influences (including variations in a shorter time scale) intact (Guo *et al.*, 2018). Figure 1 shows an example of the data stored in the database. In the top panel, the blue line corresponds to the hourly averaged RAD dose rate, whereas the red trace is the sol-filtered dose rate. The bottom panel (green line) depicts the diurnal variation of this period which seems to be about $\approx 3.5\%$.

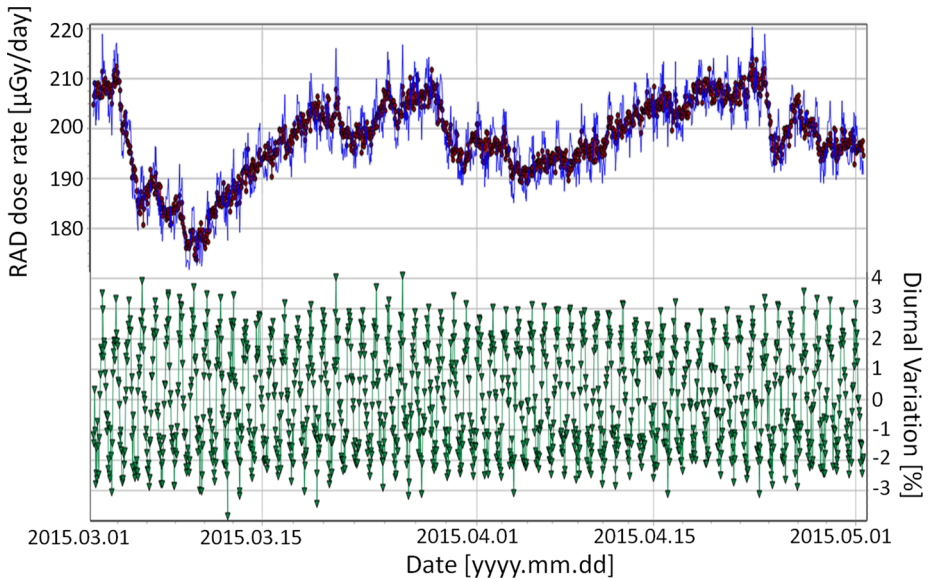


Figure 1 A sample of the RAD dose rate [$\mu\text{Gy}/\text{day}$] for a two month period, namely 01 March–30 April 2015, as those are stored in the dedicated database of FDs on the Martian soil. See text for explanations.

3.1.2. Selection

Next, we extracted FDs using hourly variations ($\delta(t)$) obtained from the sol-filtered data. Those are closest to the CR density variations obtained from the NM network data when applying the global survey method (GSM) (Belov *et al.*, 2018). GSM takes into account the recordings of all NMs of the worldwide network and provides a continuous time series of 10 GV GCR density and anisotropy outside the atmosphere and the magnetosphere. These products are used as the basis for the terrestrial FD database (Belov, 2009; Papaioannou *et al.*, 2010). We have, automatically, spotted all decreases in the RAD dose counting rate. This was a two step procedure. In the first step, we used a moving average function as follows: we applied a window centered on an hour of measurements, enforcing a width of 12 hours prior and 12 hours after this specific hour or measurement, resulting into a total of 25 hours. This time span (*i.e.* the 25 hours) was then used for the identification of the range of values for RAD. Consequently, a maximum (*Max*) and a minimum (*Min*) was identified in the count rate (within this window) as well as a time of maximum (t_{max}) and a time of minimum (t_{min}). The second step of this procedure was to calculate the difference $\delta = \frac{\text{Max}-\text{Min}}{\text{Max}}$ in % for each hour. If δ was $\geq 1\%$, a candidate decrease was marked. Next, we identified the t_{max} and t_{min} for the count rate of a candidate event that was identified. It was further assumed that t_{max} was the actual start of the candidate FD, while the t_{min} was left open and was reevaluated at every hour. All these decreases were listed as possible candidates of FD events. The next and main step was to visually inspect and to cross-check the candidate FD event with respect to its solar origin (see Section 3.1.3) and the associated FD at Earth (if any). This procedure has led to a clear sample of 424 FDs identified in the measurements of RAD on the surface of Mars. Figure 2 depicts the long term behavior of the sol-filtered RAD data for the whole time span of the database. FDs with large amplitude ($A_M > 4\%$) are noted with vertical red arrows. Red circles denote FD events that have been identified both at Earth and at Mars.

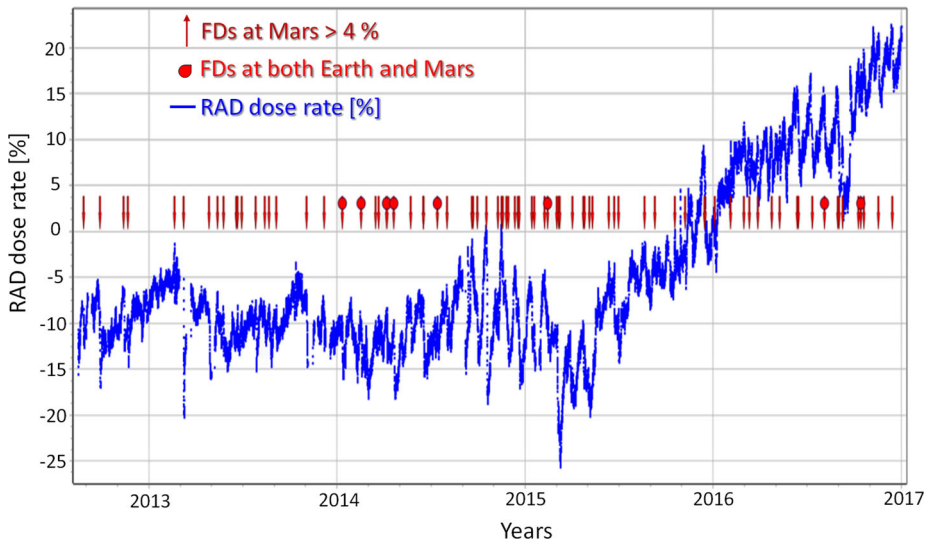


Figure 2 Long term behavior from 2012 to 2016 of the filtered Martian CR detector (*e.g.* RAD) count rate variations (*blue line*). Forbush decreases with a magnitude $> 4\%$ on the surface of Mars are pointed with *red arrows*. The *circles* identify FDs observed on both Mars and Earth.

Given the fact that the most important parameter in FDs is the magnitude of the decrease, we have also identified the maximum difference of the variations in the selected period (*i.e.* FD duration time) as $A_M = \delta$. For each of the 424 FD events we further determined a quality index (q), with respect to its identification with $q \in [1, 5]$. The highest number, 5, was assigned to those FD events in which the $\delta(t)$ data were complete, diurnal variations (Rafkin *et al.*, 2014) were reliably excluded, and there were no other difficulties in the selection of the FD and the correct determination of its size (A_M). On the other hand, the lowest number, 1, was assigned to those periods in which the selection of the FD was practically impossible for a number of reasons (*e.g.* data gaps, the effect of solar CR, unfiltered diurnal or semi-diurnal wave). The in-between ranking allocated number 2 to FD events for which it was possible to select the FD, but the size of the FD was unreliable due to data problems (*e.g.* data gaps, diurnal variation – especially prior and after a data gap). Intermediate cases with significant and minor data problems were marked cases 3 and 4, respectively.

3.1.3. Solar Origins of the Event

For each FD event recorded on Mars we tried to identify its corresponding solar source and when possible the related causative CME. For this purpose, we utilized the catalog of CMEs (Gopalswamy *et al.*, 2009) based on recordings from the *Large Angle and Spectrometric Coronagraph* (LASCO: Brueckner *et al.* 1995) onboard the *Solar and Heliospheric Observatory* (SOHO) (Domingo, Fleck, and Poland, 1995), available at https://cdaw.gsfc.nasa.gov/CME_list/ and the ICME simulations from the Wang–Sheeley–Arge (WAS) ENLIL cone model (Arge and Pizzo, 2000; Arge *et al.*, 2004) available at <https://iswa.gsfc.nasa.gov/IswaSystemWebApp/>. Furthermore, we included a quality index (q_S), ranging from 1 to 5, based on the evaluation of the identified relation. The higher the number (*i.e.* 5) corresponds to the more concrete association. A similar index is also used in the database of terrestrial

FDs maintained by IZMIRAN (Belov *et al.*, 2018). The purpose of such an index is to provide a quantification on the estimations made during the identification of the solar sources. Naturally, there are straightforward as well as complex cases. This index (as any other one) provides different levels of such an evaluation and is subjective. Every effort has been made in order to identify the most likely situation as concerns the driving solar sources. The information tabulated in Table 1 (see the Appendix) further encourages the research efforts and paves the way for the identification of more complex situations.

Additionally, we established one more index: q_E also on a five-point scale, which characterizes the quality of the association of the Martian FD to the FD event at Earth. If the identified FD events (at Mars and at Earth) were driven by the same interplanetary disturbance and no other causative event could significantly affect CRs we assigned number 5. If factors that could mask the relation of the recordings at Mars and Earth were present but their influence turned out to be rather small then q_E was set to 4. In the cases the influence was distinguishable and/or rather clear q_E was 3 and 2, respectively. If the recorded variations at Earth and Mars are totally unrelated then $q_E = 0$, at the same time a very weak or even doubtful relation is marked with $q_E = 1$.

Table 1 (see the Appendix) includes the following information: column one provides the number of the FD event, column two gives the date and column three the start time of the FD at Mars. Next, column four provides the magnitude of the FD at Mars (A_M), in %. The following three columns (*i.e.* five, six, and seven) show the assigned quality indices, q , q_S , and q_E . As a comparison, we also provide the magnitude of the FD at Earth (A_E), in %, in column eight. Note that when an FD was spotted in the RAD data but no FD was identified in the NM data – based on the solar origin of the events – we use *NULL* as a flag. This flag is also used when no data or information are available, across Table 1. Column nine provides the time from the onset of the FD event until its density minimum, t_{\min} , in [hrs]. Columns 10 and 11 show the maximal hourly decrease (*i.e.* maximum steepness) in the CR density D_{\min} in %, and the corresponding time of the maximal hourly density decrease during the main phase of the FD, tD_{\min} in [hrs], respectively.² These FD characteristics are calculated for the FDs recorded on the surface of Mars. The final four columns (*i.e.* 12, 13, 14, and 15) give the associated solar event. In particular, the launch date and time of the CME as it first appeared in LASCO-C2 onboard SOHO (columns 12 and 13, respectively), the corresponding radial linear speed of the CME, in [km/s], as this was derived by the CDAW CME catalog (column 14), and the transit velocity of the ICME from the Sun to Mars, in [km/s] (column 15), calculated based on the aforementioned timing.

Figure 3 provides a compilation of several snapshots of the capabilities offered by the database of the RAD data.

3.2. Examples of FD Events at Mars and at Earth

3.2.1. Driven by the Same ICME

Multipoint simultaneous observations of GCRs on Earth and on Mars provide unprecedented opportunities for the analysis of the impact of the interplanetary counterparts of ICMEs on GCRs. Given the relative close radial difference between the Earth (1 AU) and Mars (≈ 1.5 AU), if an ICME passes over the Earth, there is a significant probability that this interplanetary disturbance will also arrive at Mars and *vice versa* provided that the planets have a small longitudinal separation. However, this is not a one-to-one relation and each

²Details as regards the different indices and their definition can be found at Abunina *et al.* (2013b).

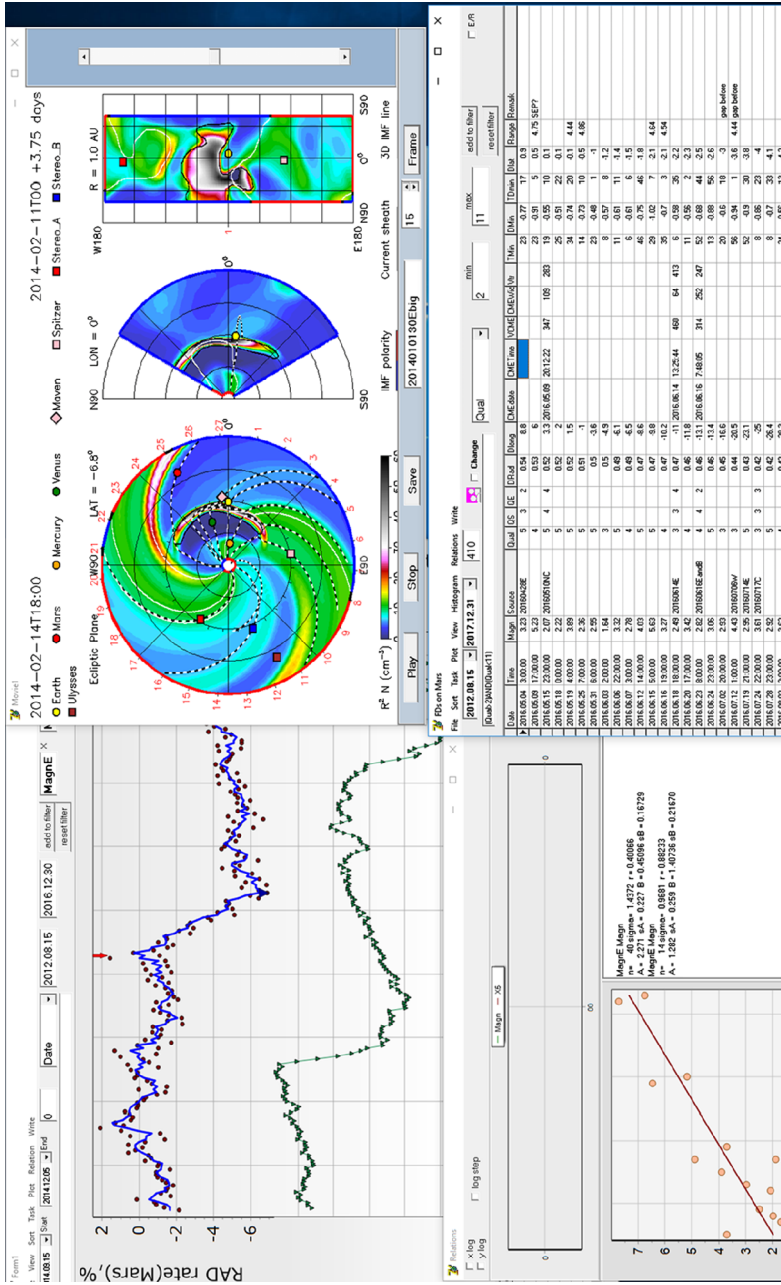
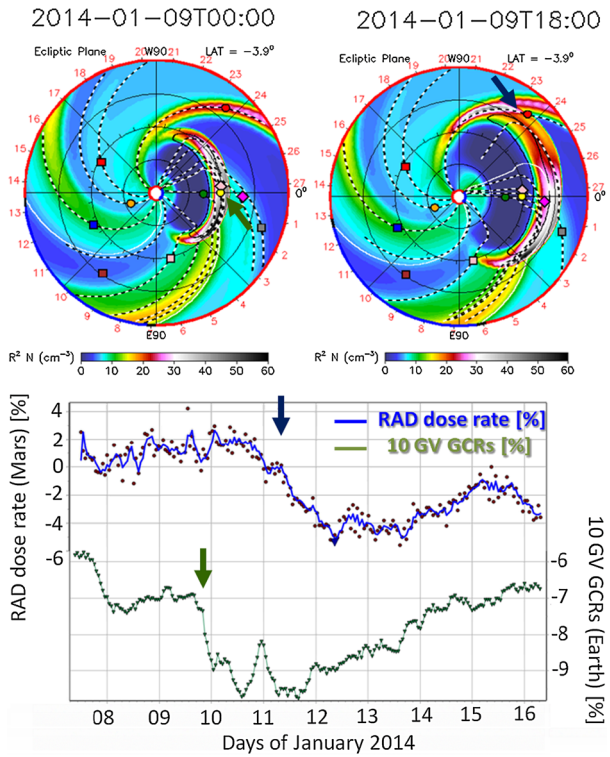


Figure 3 A compilation of snapshots of the capabilities offered by the database of FDs at Mars. The top panel on the right shows a comparison of the RAD filtered dose rate (in blue) with the output of the GSM (in green) for an indicative time range. The top panel on the right, demonstrates the related WSA ENLIL simulation with respect to the selected time range, which is also available through the database. The bottom panel on the right depicts the compiled FD database while the bottom panel on the left shows the statistics (e.g. regressions) that are possible to do in the implemented machinery.

Figure 4 WSA ENLIL model simulation of the ICME on January 2014 (*top panel*) and the resulting FDs at Mars and Earth (*bottom panel*). The *top panel* on the *left hand side* depicts the arrival of the ICME at Earth (highlighted by a *green arrow*), while the *top panel* on the *right hand side* presents the arrival of the ICME at Mars (highlighted by a *blue arrow*). The corresponding times of shock arrival are indicated in the *bottom panel* as *green* (Mars) and *blue* (Earth) *arrows* at the *top* of each of the respective time series.



case should be studied independently. ICMEs with large widths often affect at least one of the observation points, *i.e.* Mars and/or Earth. In this work, we are mostly interested in those ICMEs that resulted in a FD both on Earth and on Mars. Several examples of such events are presented in Freiherr von Forstner *et al.* (2018) and a similar example is illustrated in Figure 4.

Figure 4 shows the example of an ICME taking place in January 2014. Earth encountered the propagating ICME first and the recorded FD was recorded on 09 January 2014 at 20:00 UT. Almost 36 hours later, Mars also encountered the ICME and a FD was recorded on 11 January 2014 at 08:00 UT (see the vertical arrows in Figure 4, bottom panel). During this event, the longitudinal separation between Earth and Mars was $\approx 50^\circ$, nevertheless the ICME affected both observational points. The causative of the FD at both Mars and Earth was a fast halo CME ($V_{CME} = 1830 \text{ km s}^{-1}$) that was spotted by LASCO onboard SOHO on 07 January 2014 at 18:24 UT. In order to better understand the heliospheric variability of this period we further turned to the WSA ENLIL simulations. According to the space weather Database of Notifications, Knowledge, Information (DONKI) (<https://kauai.cmc.gsfc.nasa.gov/DONKI/view/CMEAnalysis/4364/2>), this CME resulted into an ICME with a predicted shock arrival time at Earth on 09 January 2014 at 00:38 UT and at Mars almost 17 hours later at 17:55 UT. As illustrated in the top panel on the left hand side of Figure 4, Earth encounters the central part of the ICME while Mars was influenced mainly by its edge (top panel, right hand side). As a result, the FD at Earth is characterized by a relatively fast and sharp decrease, followed by a recovery period of several days.

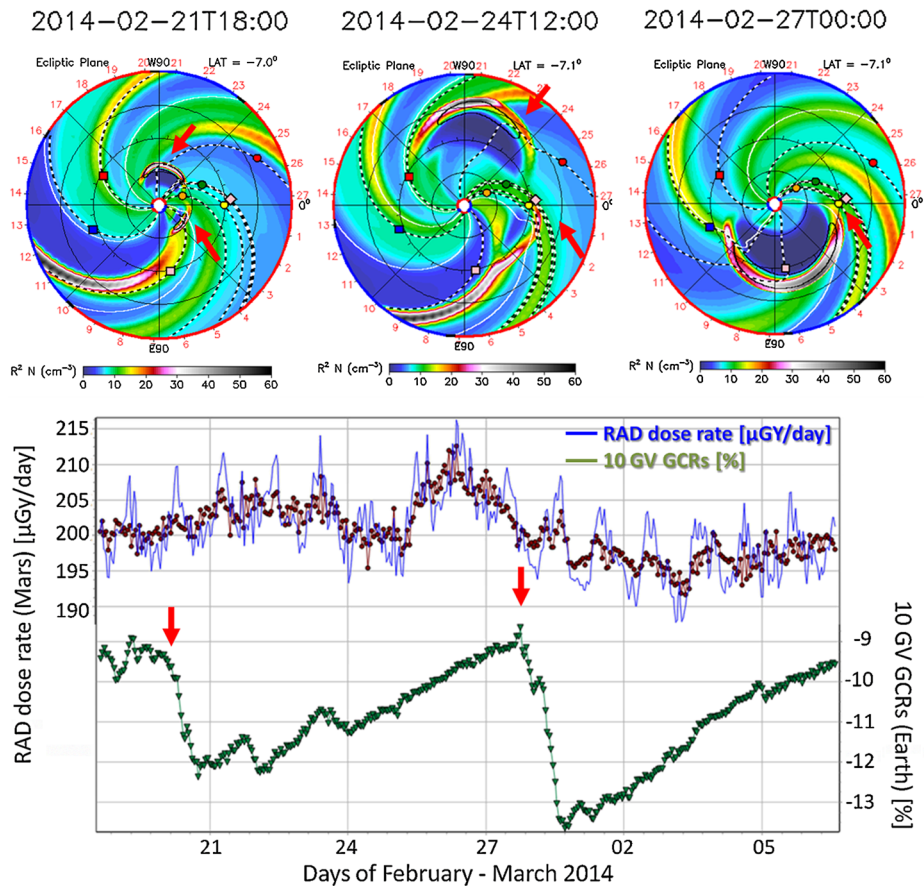


Figure 5 The WSA ENLIL simulation of the first ICME on February 2014 (*top left hand and middle panels*), the resulted CR variations on Mars and Earth in February 2014 (*bottom panel*) and the WSA ENLIL simulation of the second ICME on February 2014 (*top right hand panel*) that resulted into the large FD at Earth on 27 February 2014. The *red arrows* indicate the extension of the ICMEs in the upper WSA ENLIL panels and the start of the related FDs in the *bottom panel*.

3.2.2. Driven by Different ICMEs

In our catalog of FDs at Mars (see Table 1), we have identified examples of large ICMEs that resulted into FDs at both points in the heliosphere (*e.g.* Mars and Earth) at much larger longitudinal differences (in two cases this longitudinal difference is $> 90^\circ$).

On the other hand, there are also examples when, although the longitudinal difference is relatively small and the FDs at Earth and Mars are closely related in time, those are triggered by different ICMEs. Such an example is presented in Figure 5.

The FD started at Mars on 26 February 2014 at 09:00 UT. This was associated to a western (S15W73) relatively fast CME ($V_{\text{CME}} = 948 \text{ km s}^{-1}$) which did not encounter the Earth. At the same time a small but efficient ICME, driven by a partial halo CME of moderate velocity ($V_{\text{CME}} = 582 \text{ km s}^{-1}$) – which apparently does not affect Mars – arrived at Earth earlier and resulted into a large FD that started on 20 February 2014 (Figure 5, upper panel on left hand and middle panels, depicts this ICME in the WSA ENLIL simulations). Addi-

tionally, the bottom panel of Figure 5 presents the time evolution of the RAD dose rate at Mars (in blue color) and the 10 GV GCRs variation at Earth (in green color). The evolution of this ICME spans up until the recovery of the FD at Earth. The flank of the ICME passing by Earth and not affecting Mars can also be seen in Figure 5 (upper middle panel). However, the most significant effect during this period begins on Earth at the end of 27 February 2014 at 16:50 UT. This is associated to a large and fast ($V_{\text{CME}} = 2147 \text{ km s}^{-1}$) eastward halo CME (Figure 5, right hand panel), which occurred on 25 February 2014 at 01:25 UT, which was associated to an X4.9 flare at 00:39 UT, situated at S12E82. This ICME also passed by the east of Mars. It should be noted that February 2014 constitutes a special period, since it is one of the rare intervals for which identifications of the propagating ICME(s) were made *in situ* at different vantage points within the heliosphere (*i.e.* Mercury, Earth, Venus) (Wang *et al.*, 2018; Winslow *et al.*, 2018). These studies focus mostly on the period from 15–21 February 2014 (as concerns the ICME), which precedes the period discussed here but provides comprehensive background information for the complex conditions of the interplanetary space.

3.2.3. Complex Cases

Different combinations of structures propagating in the IP space resulted into noticeable short term GCRs intensity decreases at both Mars and Earth. In particular, interactions of: i) successive CMEs (Burlaga, Plunkett, and St. Cyr, 2002; Lugaz and Farrugia, 2014; Temmer *et al.*, 2012), ii) CMEs with HSS and/or CIRs and iii) very complex cases with more than one of the aforementioned interactions taking place. Evidently, such interaction(s) imply a significant energy and momentum transfer with the interacting flux systems being merged (Burlaga *et al.*, 2003; Liu *et al.*, 2012) and with the CMEs being deflected from their initial propagation direction (Zhuang *et al.*, 2017). The identification and interpretation of such complex events is not a trivial task since the resulting properties (*e.g.* FD amplitude) can be modified depending on relations between types and parameters of the participating structures. In our catalog of FDs at Mars, several such cases are present. For example, the events N° 135 and 136 (see Table 1) on 17 and 19 February 2014, respectively. A very complex situation with a CME-CME interaction and an additional influence of a HSS took place (Figure 6). A series of slow partial halo and halo CMEs were ejected on 11 and 12 February 2014, respectively. The fastest partial halo CME on 11 February 2014 was the one registered at LASCO-C2 on 19:24 UT (613 km s^{-1}), while the fastest halo CME on 12 February 2014 was observed at 16:36 UT (533 km s^{-1}). This halo CME propagated under disturbed conditions. This halo CME seemed to interact with the preceding CMEs, forming a larger disturbance which propagated out until Mars. Finally, Mars was under the influence of this structure until 20 February 2014 (Figure 6). Table 1, lists the FD at Mars on 17 February 2014 at 07:00 UT with an amplitude of $A_M = 6.8\%$. This is associated to the halo CME of 12 February 2014 (which is, of course, part of the overall disturbance) and then lists for Earth an FD with amplitude $A_E = 4.3\%$. This corresponds to the FD at Earth that was registered earlier on 15 February 2014 (see Figure 6).

Another complex case appears also for the events N° 175 and 176 (see Table 1) on 05 and 06 July 2014. Interaction between each of the involved CMEs (see Table 1) and a propagating HSS took place, together with the interaction and merging of the CMEs at $\approx 0.8 \text{ AU}$.³ In particular, the CME on 01 July 2014 at 11:48 UT (614 km s^{-1}) seemed to overtake the propagating ICME. However, due to the relative position of Mars with respect to the Sun

³<http://helioweather.net/archive/2014/07/>.

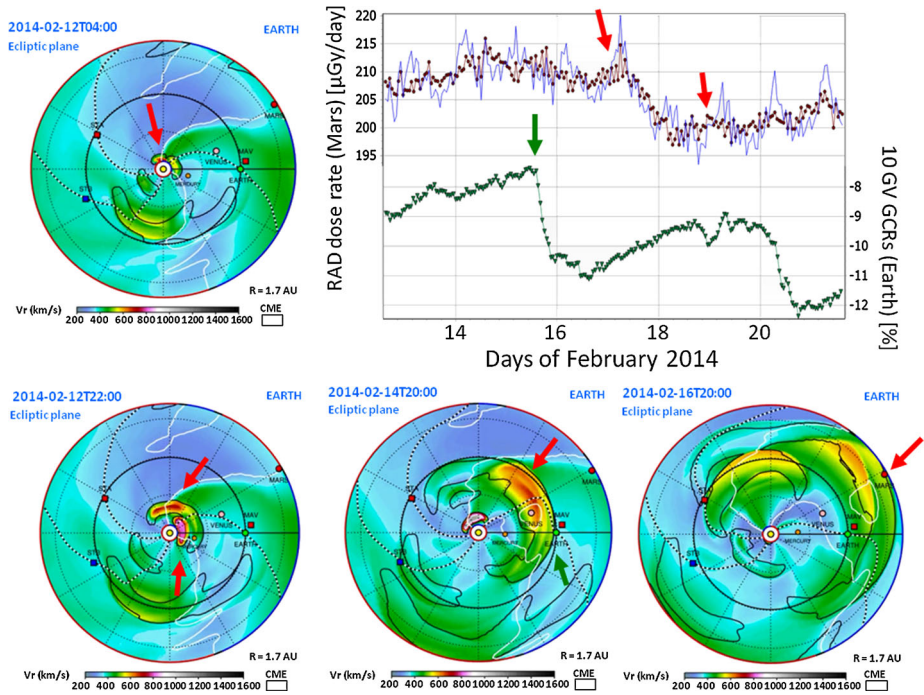


Figure 6 The WSA ENLIL and DONKI HELCATS simulation of the CME on 11 February 2014 (*top left hand panel*), the WSA ENLIL and DONKI HELCATS simulation of the second CME on 12 February 2014 (*bottom left hand panel*), their interaction as those propagate in the IP space (*bottom middle panel*), the WSA ENLIL and DONKI HELCATS simulation of the complex structure that occupied Mars up until 20 February 2014 (*bottom right hand panel*) and the resulted CR variations on Mars and Earth (*top right hand panel*). The *red arrows* indicate the extension of the CMEs and ICMEs in the WSA ENLIL and DONKI HELCATS panels and the start of the related FDs at Mars in the *top right hand panel*. The *green arrow* points to the relevant FD that was recorded at Earth.

and the eastern direction of the CMEs, Mars only encountered their flanks. As a result, a series of small amplitude (A_M) FDs were recorded at Mars.

4. Statistics

At a first glance, the FDs recorded on the surface of Mars and at Earth are surprisingly similar. Given the fact that Mars and Earth are very close, on the scale of the solar system, the interplanetary disturbances affecting both of them should be similar and there will be times that the same disturbance affects both planets. However, such similarity is still surprising, since the terrestrial and the Martian CR observations differ not less than two orders on the efficient energy of the recorded particles.

Before comparing FDs on Earth and on Mars, we need to discuss the specific features and the details of their selection *per* dataset. In principle, differences are essential. The GSM method provides as an output hourly variations of the CR density at Earth with an accuracy of $< 0.1\%$. This feature makes it possible to select even very small (in terms of magnitude A_E) FDs that sometimes appear to have an amplitude of 0.3% , with a potential unbiased

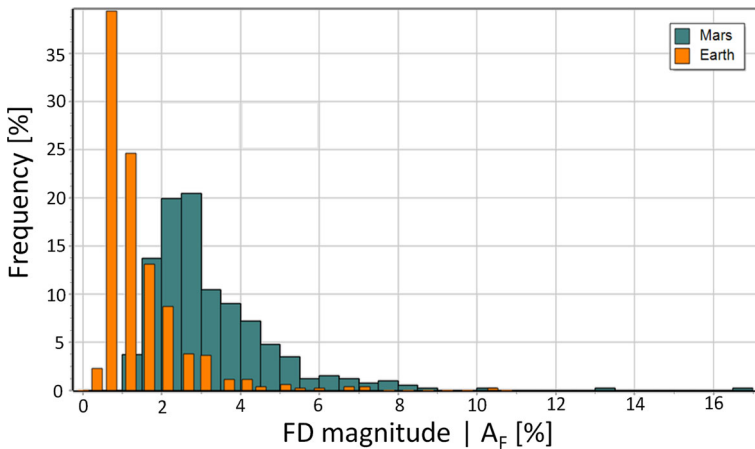
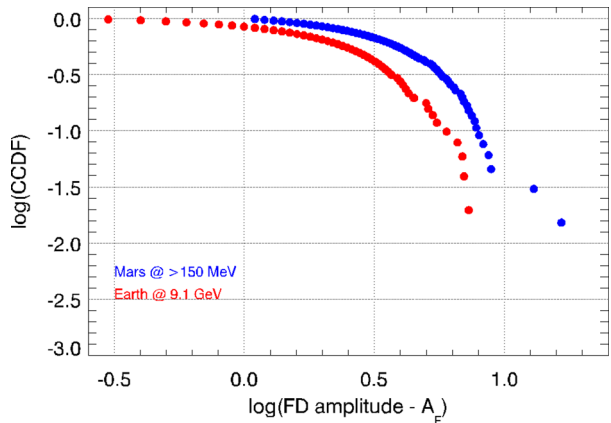


Figure 7 Distribution of the size of FDs observed in the period 2012–2016 at Earth (orange color histograms) and at Mars (blue color histograms).

selection starting at $\approx 1\%$. More important is that the GSM determines the CR characteristics separately for each hour, and this allows us to separate the density and the anisotropy variations. In addition, the near-Earth interplanetary space provides continuous measurements of all key solar wind (SW) parameters (SW velocity, intensity of the interplanetary magnetic field (IMF), and so on) and at the same time geomagnetic activity indices provide reliable identifications of the geomagnetic storms, especially the sudden storm commencements (SSCs). From the combined analysis of direct and indirect data, as a rule, it is possible to know the type of interplanetary disturbance and its arrival time at Earth. From this information one tries to get the response of the CRs (*i.e.* FD) for each interplanetary disturbance. As a result, it is possible not only to select FDs of small magnitude in the CR recordings at Earth but also to identify their solar drivers. However, this is practically impossible for the GCR data on Mars. Indeed, the smallest FDs, as concerns the magnitude (A_M), in the catalog of FDs on the surface of Mars have a size of $A_M = 1.1 - 1.2\%$. Moreover, the selection of FDs at RAD data that avoids biases starts at $\approx 3\%$ (Guo *et al.*, 2018). At the same time, RAD has given ground to the multipoint recordings of FDs on another planet, hence it provides the scientific community with unprecedented opportunities to study large scale magnetic structures (ICMEs, CIRs) propagating continuously through the interplanetary medium.

For the total time span of the Martian FD database studied here, that is, from 15 August 2012 to the end of 2016, we identified 424 FD events in the RAD dose data. During the same time period, at Earth a total of 541 events were identified. One should note that the larger number of FDs at Earth should not be misleading; if the capabilities to select the FDs from the Martian data would be similar, the number of FDs on Mars would be possibly higher compared to the relative number of FDs at Earth, because of the smaller energy of the registered CR at Mars. Furthermore, the Martian atmosphere shields away most of the GCR protons which have energies less than about 150 MeV (Guo *et al.*, 2017). This cutoff is lower than the atmospheric cutoff at Earth, which is around 450 MeV (Clem and Dorman, 2000) and the definite energy of 9.1 GeV, which corresponds to the rigidity of 10 GV used in this study. If we could use the same energy for both Earth and Mars, the resulting FDs at Mars would be smaller than at Earth, given their distance difference. FDs can be considered as the disturbances in the GCR distribution caused by local variations and the presence

Figure 8 The logarithm of the complementary cumulative distribution functions (CCDFs) versus the logarithm of the magnitude of FDs at Earth and at Mars (A_F is the magnitude of the FDs).



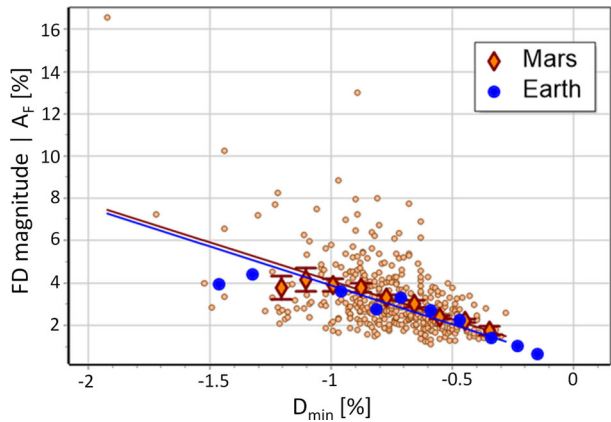
of clouds of magnetized plasma that slowly fill (Cane, Richardson, and Wibberenz, 1995; Vanhoefer, 1996; Wibberenz *et al.*, 1998; Cane, 2000; Dumbović *et al.*, 2018), hence the size of the FD will get lower for larger distances from the Sun. Furthermore, recent studies based on observational evidence have shown that the amplitude of the FD drops as a function of the heliocentric distance (Witasse *et al.*, 2017; Winslow *et al.*, 2018). However, such a comparison is beyond the scope of this article.

Figure 7 provides the distribution of the magnitude of FDs that were recorded both at the Earth (orange color histograms) and at Mars (blue color histograms). There are $n = 541$ FD events at Earth presented in this figure. However, the number of FD events at Mars is $n = 410$. This is because we used only the events with a quality index $q \geq 2$. For these two distributions the mean and the median amplitude in % for the FDs at Earth was 1.43 and 1.10, respectively. For the FDs at Mars the mean and the median amplitude in % is 3.17 and 2.74, at the respective energies at each observing point.

As a next step we compared the FDs at both planets with the same magnitude. In this comparison, the predominance of Mars is obvious: there are 341 FDs with a magnitude $> 2\%$ recorded on the Martian surface but only 106 on Earth. At the same time, if we apply the same comparison to FDs with a magnitude of $> 3\%$ the corresponding quantities are 172 and 49 for Mars and Earth, respectively. Finally, the comparison between FDs with a magnitude of $> 4\%$ leads to 92 events for Mars and 22 for Earth. The largest FD in this period was $\approx 10\%$ for the Earth, whereas on Mars the largest FD size was $> 17\%$. Referring to Figure 7, it is evident that the FDs at Mars are noticeably larger in size at the respective energies (*i.e.* $E > 150$ MeV for Mars and 9.1 GeV for Earth).

Analysis of the histograms Figure 7 reveals that the distributions of the magnitude of FDs at Earth and at Mars are highly skewed producing a long tail with large values. Distributions with such a form often follow a power law: $p(x) = Ce^{-\alpha}$. We have identified this power-law distribution by plotting the complementary cumulative distribution function (CCDF) on a log–log scale (Figure 8). The straight line asserts above some minimum values X_{\min} both for Mars and for Earth which means that the tail of the distributions appears to be a power law (Newman, 2005). The method of a linear regression is used for the estimation of the power-law slope α . The estimation of X_{\min} is based on the Kolmogorov–Smirnov statistics (Clauset, Shalizi, and Newman, 2009). The distribution of FDs at Earth corresponds to a power law slope $-\alpha = -2.40 \pm 0.19$ with $A_E \geq 1.1\%$ (284 FDs from 2012 to 2016). Similar results were obtained for terrestrial FDs from 1957 to 2016 (4692 events), $-\alpha = -2.31 \pm 0.11$, $A_E \geq 1.4\%$ (2159 FDs). As for the distribution of A_M , its power law

Figure 9 The relation between the maximal hourly decrease in the CR density (DM_{in}) and the total size of the Forbush decrease. *Small circles* represent individual episodes of FDs on Mars. *Diamonds* represent FDs on Mars averaged for equal intervals of the variation of D_{min} (standard statistical errors are also shown). *Large blue circles* are similarly averaged values of the FDs on Earth. In addition the linear regressions are presented for each sample, color coded as: *red* for FDs at Mars and *blue* for FDs at Earth. See text for details.



slope is significantly steeper and the value from which the power law begins is noticeably larger than that for the distribution of A_E (Figure 8). For the magnitude of FDs at Mars, a power-law has been identified recently by Guo *et al.* (2018) who used FD recordings on the surface of Mars (by MSL) and outside the Martian atmosphere (by the *Mars Atmosphere and Volatile Evolution Mission* (MAVEN)). For their sample of 121 FD events registered by MSL, an $\alpha = -2.08 \pm 0.32$ was obtained. However, for FDs that were registered by MSL but not by MAVEN the corresponding α was -2.85 ± 0.57 , with the spectra being less of a power-law distribution with higher uncertainties of the fitting. Hence, the identification of a reliable slope is not a trivial task. In our work, although the correspondence of the tail of the A_M distribution to a power law follows from the CCDF, we do not have enough FDs at Mars with $A_M \geq X_{min}$, at present, to reliably estimate the slope with sufficient accuracy.

Relations between different characteristics of FDs at Earth, such as the connection between the maximal hourly decrease in the CR density (DM_{in}) and the total size of the FD (A_M) have been studied by Belov (2009) and Abunin *et al.* (2012). This correlation has also been identified here for the FD events recorded on the surface of Mars (Figure 9). The circles depict the individual FD events. The diamonds of orange color represent the binned averaged intervals of the variation of D_{min} with the standard statistical errors overplotted.

For comparison, Figure 9, also presents the binned averaged intervals of variation of D_{min} in the same time period for Earth. It can be seen that the Martian and the terrestrial FDs are surprisingly well matched. In particular, for Mars the linear regression yields the following relation:

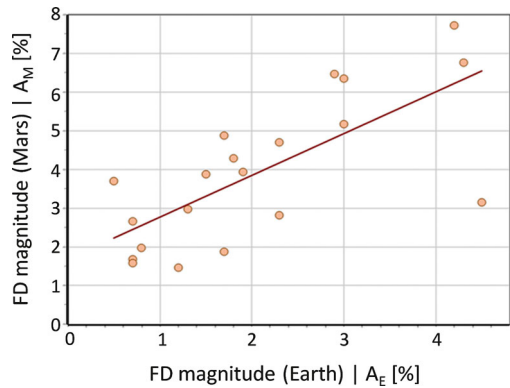
$$A_M = (0.47 \pm 0.07) + (-3.64 \pm 0.32) \cdot D_{min}. \tag{1}$$

At the same time, a similar regression is obtained for Earth:

$$A_E = (0.20 \pm 0.03) + (-3.69 \pm 0.16) \cdot D_{min}. \tag{2}$$

It is most interesting to compare FDs observed at Earth and at Mars that are triggered by the same solar source (*i.e.* ICME). This is because it is possible to derive the propagation time of the ICME in the interplanetary space as well as its corresponding deceleration (or acceleration). Furthermore, multipoint observations of FDs at Earth and at Mars can be used to quantify the actual effect of the ICMEs on the radiation environment of each observing point. Such events constitute a rather small part over the whole sample of events.

Figure 10 Relation of the magnitudes for FDs caused by the same interplanetary disturbances on Earth and on Mars.



Nevertheless, in these four and a half years of continuous measurements at Mars several tens of events were identified. In particular, we applied the following criteria: $3 < q \leq 5$ and $2 < q_E \leq 5$ in our database of FD events at Mars. This is because we wanted to retrieve a sample of FD events with a high quality index for both the identification of the FD event (q) at Mars and its relation to FDs at Earth (q_E). As a result, a sample of $n = 20$ FD events recorded at both Mars and Earth was identified. For these events we compared the magnitude of the FD at Earth to the one at Mars (Figure 10). The correlation coefficient was $cc = 0.71$.

The linear regression overplotted in Figure 10, yields the following relation:

$$A_M = (1.07 \pm 0.24) \cdot A_E + (1.7 \pm 0.3). \quad (3)$$

It appears (see Figure 10) that FDs at Mars are larger in size compared to terrestrial FDs, for the respective energies at each observing point. In particular, for small effects ($< 2\%$) this difference is about 2–3 times, while for the largest events in this comparison the difference is about 1.5 times.

According to Equation 3, an ICME with no FD at Earth would have an expected FD at Mars with the noticeable amplitude of $1.7 (\pm 0.3)\%$. This is most probably due to the fact that numerous small interplanetary disturbances with weak magnetic fields can modulate CRs of low energy like those recorded by RAD on Mars, but their effect on GCR charged particles with a rigidity of 10 GV (≈ 9.1 GeV) (as those are derived by the application of the GSM on the neutron monitor data of the worldwide network) will be almost imperceptible. In general, FDs obtained from RAD dose rates at Mars obviously surpass the amplitude of the near-Earth FDs observed by neutron monitors (Figure 10), at the respective energies recorded at each observing point. If we, on top of this, consider the distinction of energies at the different observing points, we could expect significantly greater differences in the magnitudes of FDs. This is because the FDs observed at Earth are strongly dependent on the energy of the particles and their amplitude noticeably increases as a function of the decreasing energy. A recent extended study of a large number of FDs at Earth has shown that a typical (mean) index with a power-law spectrum (γ) of the dependence of the size of the FDs (A_E) (caused by ICMEs) on the rigidity (R), assuming that the spectrum of the cosmic ray variations is defined as $A_0 R^{-\gamma}$, is: $\gamma = 0.6–0.7$. This estimation

refers to a $R = 10$ GV (or equivalently to an energy of ≈ 9.1 GeV) and represents a mean value for FDs, taking into account the evolution of γ within the different phases of a FD (Klyueva, Belov, and Eroshenko, 2017). Proton energies of > 150 MeV (similar to those recorded from RAD at Mars) would fall into a range of rigidities of > 0.55 GV, hence, based on the aforementioned rigidity dependence, the expected size of the FD at Mars (A_M) would be higher than the size of the FD at Earth (A_E) not only by a factor of 1.5–2 (see above). However, this is not what we observe in the data. It should further be noted for completeness that, for RAD, located in Gale Crater, well below the mean Martian surface altitude, the atmosphere is effectively shielding against GCR particles below a cutoff energy of about 165 MeV/nuc. However, this cutoff energy also changes as the Martian atmospheric depth changes diurnally and seasonally (Rafkin *et al.*, 2014; Guo *et al.*, 2015) up to 25%. Simulations of particle transport through the atmosphere have shown that the cutoff energy varies between 140 and 190 MeV depending on the atmospheric depth which may change between 18 and 25 g/cm² during different seasons (Guo *et al.*, 2019). A possible explanation is that, during the propagation of the ICME from the Earth orbit to Mars, the efficiency of the ICME to modulate CRs decreases. At the same time, it is also likely that the energy (rigidity) dependence of the FD magnitude actually changes upon transition to lower energies. Perhaps this is due to the shape of the background energy spectrum of galactic CRs, which in the inner heliosphere has a maximum, due to the modulation of CRs by the solar wind, close to several hundreds of MeV. One should note that FDs are created at the expansion of the interplanetary disturbance (*e.g.* ICME), which is a quasi-trap for the charged CR particles (Parker, 1965; Belov, 2009). During the expansion, GCR particles are cooling (*i.e.* lose energy). If the CR spectrum is decreasing (with increasing energy), *i.e.* CR flux drops as a function of energy, for CR particles with energies detected by neutron monitors (*e.g.* ≥ 1 GV), this leads to a decrease in the observed CR density of a given energy (rigidity). In the opposite case, if the CR spectrum is increasing (with increasing energy), *i.e.* the CR flux rises as a function of energy, for example in the energy range of up to a few hundreds MeV, the energy loss can only reduce the actual FD.

5. Conclusions

We have performed a systematic scanning of MSL/RAD dose rate recordings from 2012 to 2016. A total of 424 FDs were identified in this period, leading to a comprehensive catalog of FD events recorded on the surface of Mars. This is the largest database of FDs that has been observed away from Earth and also for measurements of relatively low energies (comparing to the observations retrieved by neutron monitors).

Furthermore, we performed a comparative statistical analysis between the FDs recorded at Mars (at $E > 150$ MeV) and at Earth (at $E = 9.1$ GeV) and we have shown that:

- FDs at Mars and Earth have almost identical dependencies on the values of the maximum hourly decrease of the CR density (DM_{in}) to the size of the FD at the respective energies (see Figure 9 and Equations 1 and 2).
- The MSL/RAD data, at an energy of $E > 150$ MeV, allow for the identification of FDs with a magnitude exceeding 1.5–2% while the mean amplitude of the identified FDs at Mars is 3.17%.

- When selecting a prime sample of FDs at Earth and at Mars, driven by the same ICME, a significant correlation ($cc = 0.71$) and a linear regression between the sizes of the FDs at the different observing points, for the respective energies at each observing point, was obtained (see Figure 10 and Equation 3).

In addition, it was shown that the FDs observed at Mars, for protons with an energy of > 150 MeV, have larger sizes (A_M) compared with terrestrial FDs. This is in line with the findings of an independent recent study of FDs (Guo *et al.*, 2018). However, it is noted that the observed differences in magnitude (Figure 10) are much smaller than what is expected from the differences in the energy ranges in both sets of observations. Most probably this is the result of the weakening of the energy dependence of the FD size at low energies, which provides evidence that the cooling of the CR particles, inside the ICME, plays an important role in the creation of FDs observed at Earth during its expansion.

Finally, we have tabulated all identified FDs at Mars from MSL/RAD in Table 1 (see the Appendix), where we also provide the start time and the magnitude of the FD (A_M). Furthermore, in the same table we present the related (if any) FDs at Earth, their sizes (A_E) and the characteristics of the FDs at Mars (*i.e.* t_{\min} , DM_{in} , tD_{\min}), as well as three quality indices that quantify the degree of the uncertainty in the identification of the FD at Mars (q), the association to an FD at Earth (q_E), and the obtained solar association (q_S). Table 1 also includes the identification of the parent solar event (*i.e.* CME) together with the relevant information derived from the SOHO/LASCO CME catalog. It is noteworthy that a comparison of the catalog of FDs on the surface of Mars presented in this work to the one reported in Guo *et al.* (2018) has an overlap of 71%, which underlines a remarkable similarity considering the independent way of establishing the lists in these two articles. We also note that all of the large FD events are present at both lists. Given the fact that several of the events that are not identical in these two catalogs correspond in principle to the same event with a difference in the identified start time, the resulted similarity would be even higher. The results of our analysis (including Table 1) can be freely utilized in future studies.

Disclosure of Potential Conflict of Interest The authors declare that they have no conflict of interest.

Acknowledgements RAD is supported by NASA (HEOMD) under JPL subcontract #1273039 to Southwest Research Institute and in Germany by DLR and DLR's Space Administration grant numbers 50QM0501, 50QM1201, and 50QM1701 to the Christian Albrechts University, Kiel. We acknowledge the NMDB database (www.nmdb.eu), founded under the European Union's FP7 programme (contract no. 213007) for providing the data. The MSL data used in this paper are archived in the NASA Planetary Data System's Planetary Plasma Interactions Node at the University of California, Los Angeles. The PPI node is hosted at <https://pds-ppi.igpp.ucla.edu/>. A quick-look of the data can be downloaded from <http://mslrad.spaceops.swri.org/beta/Home>. Simulation results have been provided by the Community Coordinated Modeling Center at Goddard Space Flight Center through their archive of real-time simulations (<https://ccmc.gsfc.nasa.gov/iswa/>). The CCMC is a multiagency partnership between NASA, AFMC, AFOSR, AFRL, AFWA, NOAA, NSF, and ONR. ENLIL with Cone Model was developed by D. Odstrcil at George Mason University. The SOHO LASCO CME catalog is generated and maintained at the CDAA Data Center by NASA and The Catholic University of America in cooperation with the Naval Research Laboratory. SOHO is a project of international cooperation between ESA and NASA. A. Anastasiadis received partial support by the PROTEAS II project (MIS 5002515), which is implemented under the "Reinforcement of the Research and Innovation Infrastructure" action, funded by the "Competitiveness, Entrepreneurship and Innovation" operational programme (NSRF 2014-2020) and is cofinanced by Greece and the European Union (European Regional Development Fund). J.G. is partly supported by the Key Research Program of the Chinese Academy of Sciences under grant no. XDPB11. AP would like to gratefully acknowledge the hospitality and the support of the IZMIRAN group that made his working visit at Troitsk possible.

Publisher's Note Springer Nature remains neutral with regard to jurisdictional claims in published maps and institutional affiliations.

Appendix

Table 1 The catalog of Forbush decreases at Mars. See text for details.

No.	Date	Time [UT]	AM [%]	q	qS	qE	AE [%]	t _{min} [hrs]	DM _{in} [%]	tD _{Min} [hrs]	CME date	CME time [UT]	V _{CME} [km s ⁻¹]	V _{transit} [km s ⁻¹]
1	2012.08.26	2:00	4.9	4	0	0	NULL	30	-0.79	3			NULL	NULL
2	2012.09.12	3:00	2.5	4	0	0	NULL	25	-0.58	33			NULL	NULL
3	2012.09.14	3:00	4	5	0	0	NULL	25	-0.73	3			NULL	NULL
4	2012.09.23	21:00	2.3	5	0	0	NULL	10	-0.62	39			NULL	NULL
5	2012.09.25	5:00	5.5	5	0	0	NULL	25	-0.63	7			NULL	NULL
6	2012.09.27	1:00	8.9	5	0	0	NULL	20	-0.97	16	2012.09.23	14:48:05	939	506
7	2012.09.28	8:00	1.8	3	0	0	NULL	5	-0.76	3			NULL	NULL
8	2012.10.01	14:00	1.8	2	0	0	NULL	17	-0.48	4			NULL	NULL
9	2012.10.02	19:00	1.5	4	0	0	NULL	8	-0.41	8			NULL	NULL
10	2012.10.03	21:00	2.6	5	0	0	NULL	8	-0.74	6			NULL	NULL
11	2012.10.05	13:00	2	4	0	0	NULL	11	-0.45	1			NULL	NULL
12	2012.10.07	3:00	1.6	4	0	0	NULL	26	-0.53	5			NULL	NULL
13	2012.10.08	0:00	2	4	0	0	NULL	11	-0.65	11			NULL	NULL
14	2012.10.13	10:00	2.9	5	0	0	NULL	25	-0.53	14			NULL	NULL
15	2012.10.15	2:00	1.3	3	0	0	NULL	9	-0.59	21			NULL	NULL
16	2012.10.17	10:00	1.4	4	0	0	NULL	5	-0.43	2			NULL	NULL
17	2012.10.19	7:00	3.5	5	0	0	NULL	13	-0.56	8			NULL	NULL
18	2012.10.21	3:00	1.8	5	0	0	NULL	20	-0.51	26			NULL	NULL
19	2012.10.27	5:00	2.1	4	0	0	NULL	10	-0.54	8			NULL	NULL
20	2012.10.28	0:00	2.5	5	0	0	NULL	20	-0.67	0			NULL	NULL
21	2012.10.30	0:00	1.5	4	0	0	NULL	17	-0.36	17			NULL	NULL
22	2012.11.02	10:00	1.4	3	0	0	NULL	25	-0.39	18			NULL	NULL

Table 1 (Continued)

No.	Date	Time [UT]	AM [%]	q	qS	qE	A _E [%]	t _{min} [hrs]	DM _{in} [%]	tD _{min} [hrs]	CME date	CME time [UT]	V _{CME} [km s ⁻¹]	V _{transit} [km s ⁻¹]
23	2012.11.04	21:00	2	3	0	0	NULL	27	-0.56	22			NULL	NULL
24	2012.11.10	2:00	1.4	4	0	0	NULL	12	-0.37	36			NULL	NULL
25	2012.11.12	17:00	7.2	5	5	2	NULL	31	-1.3	11	2012.11.08	02:36:06	855	376
26	2012.11.14	9:00	1.8	4	0	0	NULL	8	-0.48	32			NULL	NULL
27	2012.11.17	15:00	2.5	5	0	0	NULL	10	-0.51	3			NULL	NULL
28	2012.11.19	3:00	1.2	4	0	0	NULL	8	-0.6	4			NULL	NULL
29	2012.11.20	5:00	6.1	5	4	2	NULL	35	-0.63	9	2012.11.16	07:24:14	775	444
30	2012.11.22	17:00	3.3	3	0	0	NULL	9	-0.59	2			NULL	NULL
31	2012.11.24	1:00	1.5	4	0	0	NULL	23	-0.61	14			NULL	NULL
32	2012.11.29	5:00	2	4	0	0	NULL	24	-0.48	20			NULL	NULL
33	2012.12.01	13:00	3	3	0	0	NULL	38	-0.41	4			NULL	NULL
34	2012.12.07	3:00	3	4	0	0	NULL	36	-0.64	3			NULL	NULL
35	2012.12.09	17:00	2	4	0	0	NULL	11	-0.47	23			NULL	NULL
36	2012.12.10	22:00	1.8	4	0	0	NULL	24	-0.54	22			NULL	NULL
37	2012.12.12	11:00	1.3	4	0	0	NULL	14	-0.49	5			NULL	NULL
38	2012.12.14	5:00	1.9	4	0	0	NULL	33	-0.51	15			NULL	NULL
39	2012.12.16	16:00	4	4	0	0	NULL	32	-0.52	9			NULL	NULL
40	2012.12.20	2:00	3.3	4	0	0	NULL	15	-0.82	28			NULL	NULL
41	2012.12.21	2:00	2.1	4	0	0	NULL	20	-0.81	4			NULL	NULL
42	2012.12.22	21:00	1.6	4	0	0	NULL	17	-0.41	1			NULL	NULL
43	2012.12.26	5:00	3.7	5	0	0	NULL	26	-0.71	10			NULL	NULL
44	2013.01.01	4:00	2.8	4	0	0	NULL	29	-0.47	5			NULL	NULL
45	2013.01.05	14:00	2.2	4	0	0	NULL	23	-0.88	21			NULL	NULL
46	2013.01.08	8:00	1.6	4	0	0	NULL	13	-0.36	24			NULL	NULL

Table 1 (Continued)

No.	Date	Time [UT]	ΔM [%]	q	q_S	q_E	A_E [%]	t_{min} [hrs]	DM_{in} [%]	tD_{min} [hrs]	CME date	CME time [UT]	V_{CME} [$km\ s^{-1}$]	$V_{transit}$ [$km\ s^{-1}$]
47	2013.01.12	13:00	2	5	0	0	NULL	34	-0.6	12			NULL	NULL
48	2013.01.16	8:00	2.8	4	0	0	NULL	33	-0.5	3			NULL	NULL
49	2013.01.23	16:00	2	4	0	0	NULL	10	-0.55	1			NULL	NULL
50	2013.01.25	22:00	2.3	4	0	0	NULL	20	-0.4	1			NULL	NULL
51	2013.01.27	17:00	1.9	3	0	0	NULL	19	-0.83	12			NULL	NULL
52	2013.02.02	14:00	1.8	4	0	0	NULL	29	-0.41	18			NULL	NULL
53	2013.02.09	0:00	2.2	3	0	0	NULL	26	-0.6	0			NULL	NULL
54	2013.02.12	4:00	1.7	3	0	0	NULL	23	-0.39	21			NULL	NULL
55	2013.02.18	17:00	6.5	3	0	0	NULL	12	-1.43	5			NULL	NULL
56	2013.03.08	5:00	16.6	4	0	0	NULL	28	-1.92	7	2013.03.05	03:48:05	1316	568
57	2013.03.12	10:00	1.8	4	0	0	NULL	9	-0.5	7			NULL	NULL
58	2013.03.22	21:00	2.6	3	0	0	NULL	24	-0.68	23			NULL	NULL
59	2013.03.26	21:00	3.4	4	0	0	NULL	16	-0.43	14			NULL	NULL
60	2013.03.30	5:00	2.6	4	0	0	NULL	50	-0.28	48			NULL	NULL
61	2013.04.03	20:00	2.3	4	0	0	NULL	9	-0.4	49			NULL	NULL
62	2013.04.08	13:00	2.8	4	0	0	NULL	36	-0.49	0			NULL	NULL
63	2013.04.13	0:00	1.8	3	0	0	NULL	34	-0.32	24			NULL	NULL
64	2013.04.17	2:00	1.6	4	0	0	NULL	12	-0.49	52			NULL	NULL
65	2013.04.19	14:00	2.9	4	0	0	NULL	45	-0.69	2			NULL	NULL
66	2013.04.26	20:00	1.5	4	0	0	NULL	14	-0.3	3			NULL	NULL
67	2013.04.27	14:00	7.8	5	4	0	NULL	39	-0.68	36	2013.04.24	00:48:05	699	488
68	2013.05.08	21:00	2.8	4	0	0	NULL	5	-0.93	3			NULL	NULL
69	2013.05.13	19:00	4.9	4	0	0	NULL	69	-0.98	9			NULL	NULL
70	2013.05.25	6:00	4.9	5	5	0	NULL	17	-0.64	6	2013.05.22	13:25:50	1466	636

Table 1 (Continued)

No.	Date	Time [UT]	AM [%]	q	qS	qE	A _E [%]	t _{min} [hrs]	DM _{in} [%]	tD _{Min} [hrs]	CME date	CME time [UT]	V _{CME} [km s ⁻¹]	V _{transit} [km s ⁻¹]
71	2013.05.26	16:00	2.1	3	3	1	NULL	21	-0.59	19			NULL	NULL
72	2013.06.01	10:00	3	4	0	0	NULL	7	-0.83	74			NULL	NULL
73	2013.06.05	7:00	2.5	5	0	0	NULL	19	-0.64	3			NULL	NULL
74	2013.06.14	2:00	3.3	4	0	0	NULL	57	-0.48	14			NULL	NULL
75	2013.06.18	21:00	5	4	0	0	NULL	6	-0.88	57			NULL	NULL
76	2013.06.21	20:00	4.2	5	4	0	NULL	33	-0.96	13	2013.06.16	20:24:05	442	346
77	2013.06.23	21:00	4	3	0	0	NULL	21	-0.73	1			NULL	NULL
78	2013.06.29	14:00	4.1	5	5	0	NULL	18	-0.63	15	2013.06.24	04:00:05	709	319
79	2013.07.01	6:00	2.2	4	4	0	NULL	34	-0.69	4	2013.06.25	11:12:05	349	299
80	2013.07.03	5:00	2.1	4	4	0	NULL	10	-0.88	36			NULL	NULL
81	2013.07.06	10:00	1.9	3	0	0	NULL	17	-0.6	27			NULL	NULL
82	2013.07.10	21:00	1.9	3	0	0	NULL	22	-1.02	14			NULL	NULL
83	2013.07.15	14:00	2.3	4	0	0	NULL	11	-0.67	26			NULL	NULL
84	2013.07.17	23:00	2.4	5	-1	0	NULL	13	-0.97	3			NULL	NULL
85	2013.07.19	18:00	4	4	-1	-1	NULL	25	-1.01	4			NULL	NULL
86	2013.07.24	3:00	2.3	4	0	0	NULL	4	-0.82	3			NULL	NULL
87	2013.07.27	6:00	8.3	5	5	0	NULL	20	-1.22	12	2013.07.22	06:24:05	1004	350
88	2013.08.03	2:00	1.8	3	0	0	NULL	35	-0.76	30			NULL	NULL
89	2013.08.11	15:00	2.2	3	0	0	NULL	32	-0.44	18			NULL	NULL
90	2013.08.13	10:00	4.2	4	3	0	NULL	25	-0.79	36	2013.08.06	16:24:05	309	257
91	2013.08.15	17:00	2.8	4	0	0	NULL	6	-0.73	3			NULL	NULL
92	2013.08.17	6:00	1.8	4	4	1	NULL	25	-0.99	23	2013.08.10	09:48:05	415	252
93	2013.08.21	22:00	4.3	5	NULL	0	NULL	41	-0.6	47			NULL	NULL
94	2013.08.24	20:00	4.6	3	4	0	NULL	40	-0.89	4	2013.08.19	23:12:11	877	354

Table 1 (Continued)

No.	Date	Time [UT]	ΔM [%]	q	q_S	q_E	A_E [%]	t_{min} [hrs]	DM_{in} [%]	tD_{min} [hrs]	CME date	CME time [UT]	V_{CME} [$km\ s^{-1}$]	$V_{transit}$ [$km\ s^{-1}$]
95	2013.08.29	5:00	1.7	2	0	0	NULL	9	-0.38	25			NULL	NULL
96	2013.09.02	12:00	2.8	4	3	0	NULL	32	-0.77	31	2013.08.28	15:48:05	580	358
97	2013.09.04	21:00	5.3	5	3	0	NULL	33	-1.1	9	2013.08.30	18:24:05	446	337
98	2013.09.10	23:00	1.8	3	0	0	NULL	7	-0.5	21			NULL	NULL
99	2013.09.15	16:00	2.4	3	0	0	NULL	19	-1.18	17			NULL	NULL
100	2013.09.19	11:00	2.6	3	0	0	NULL	17	-0.86	3			NULL	NULL
101	2013.09.24	13:00	2.3	3	0	0	NULL	5	-0.78	3			NULL	NULL
102	2013.09.25	6:00	3.3	4	0	0	NULL	24	-0.9	3			NULL	NULL
103	2013.10.01	22:00	1.7	3	0	0	NULL	8	-0.44	3			NULL	NULL
104	2013.10.04	12:00	1.4	3	3	2	4.2	10	-0.53	6	2013.09.29	22:12:05	1179	378
105	2013.10.07	3:00	2.1	4	0	0	NULL	3	-0.73	3			NULL	NULL
106	2013.10.10	1:00	3.1	4	5	0	NULL	18	-0.89	6	2013.10.02	20:36:05	619	241
107	2013.10.12	5:00	2.5	3	0	0	NULL	8	-0.66	7			NULL	NULL
108	2013.10.12	20:00	4	3	0	0	NULL	10	-0.77	3			NULL	NULL
109	2013.10.13	23:00	3.9	2	0	0	NULL	9	-1.22	7			NULL	NULL
110	2013.10.15	1:00	3.6	2	0	0	NULL	13	-1.14	9			NULL	NULL
111	2013.10.22	1:00	3.1	2	0	0	NULL	12	-1.02	10			NULL	NULL
112	2013.10.24	10:00	4.4	3	0	0	NULL	15	-0.9	9			NULL	NULL
113	2013.11.02	13:00	6.1	4	4	2	NULL	33	-0.87	28	2013.10.27	12:12:06	525	275
114	2013.11.03	23:00	3.8	2	0	0	NULL	14	-0.94	3			NULL	NULL
115	2013.12.04	19:00	2.3	4	0	0	NULL	29	-0.86	29			NULL	NULL
116	2013.12.06	12:00	4.7	5	0	0	NULL	7	-1.04	5			NULL	NULL
117	2013.12.08	16:00	3.5	4	0	0	NULL	222	-0.54	1			NULL	NULL
118	2013.12.18	8:00	2.8	3	0	0	NULL	10	-0.81	8			NULL	NULL

Table 1 (Continued)

No.	Date	Time [UT]	AM [%]	q	q_S	q_E	A_E [%]	t_{min} [hrs]	DM_{in} [%]	tD_{Min} [hrs]	CME date	CME time [UT]	V_{CME} [$km\ s^{-1}$]	$V_{transit}$ [$km\ s^{-1}$]
119	2013.12.25	7:00	3.8	4	0	0	NULL	22	-0.85	5			NULL	NULL
120	2013.12.30	23:00	2.7	4	0	0	NULL	13	-0.59	11			NULL	NULL
121	2014.01.03	2:00	2.3	4	0	0	NULL	7	-0.68	2			NULL	NULL
122	2014.01.09	14:00	2.3	5	3	2	NULL	5	-0.97	2	2014.01.04	23:12:05	567	375
123	2014.01.10	18:00	2.3	5	4	0	NULL	8	-0.54	7	2014.01.06	08:00:05	1402	392
124	2014.01.11	8:00	5.2	5	4	5	3	25	-0.72	3	2014.01.07	18:24:05	1830	485
125	2014.01.15	8:00	2.6	5	NULL	NULL	NULL	25	-0.75	4			NULL	NULL
126	2014.01.27	9:00	2.6	4	NULL	NULL	NULL	35	-1.21	4			NULL	NULL
127	2014.01.28	21:00	3.1	4	NULL	NULL	NULL	25	-0.97	4			NULL	NULL
128	2014.01.31	20:00	2.4	3	0	0	NULL	22	-0.67	0			NULL	NULL
129	2014.02.02	10:00	2.9	3	0	0	NULL	38	-1.02	42			NULL	NULL
130	2014.02.06	18:00	3.7	4	NULL	NULL	NULL	23	-0.76	35			NULL	NULL
131	2014.02.08	2:00	3.9	4	4	4	1.5	36	-0.82	34	2014.02.04	01:25:46	528	430
132	2014.02.10	1:00	2	3	0	0	NULL	6	-0.51	24			NULL	NULL
133	2014.02.12	10:00	2.2	3	0	0	NULL	10	-0.54	29			NULL	NULL
134	2014.02.14	16:00	3.5	4	0	0	NULL	39	-1.02	30			NULL	NULL
135	2014.02.17	7:00	6.8	5	5	5	4.3	24	-0.8	15	2014.02.12	16:36:05	533	376
136	2014.02.19	1:00	1.6	5	3	0	NULL	11	-0.41	11	2014.02.11	19:24:05	613	239
137	2014.02.23	9:00	3	4	4	5	1.3	17	-0.88	4	2014.02.18	01:36:21	779	324
138	2014.02.24	5:00	1.7	4	4	5	0.7	6	-0.51	5	2014.02.19	04:48:05	612	346
139	2014.02.26	9:00	5.3	5	5	1	NULL	34	-0.78	10	2014.02.20	08:00:07	948	287
140	2014.02.28	17:00	3.2	4	2	2	5.5	6	-0.88	2	2014.02.25	01:25:50	2147	475
141	2014.03.03	23:00	2.5	3	0	0	NULL	15	-0.76	19			NULL	NULL
142	2014.03.08	14:00	2.6	4	0	0	NULL	13	-0.84	11			NULL	NULL

Table 1 (Continued)

No.	Date	Time [UT]	AM [%]	q	q _S	q _E	A _E [%]	t _{min} [hrs]	DM _{in} [%]	tD _{Min} [hrs]	CME date	CME time [UT]	V _{CME} [km s ⁻¹]	V _{transit} [km s ⁻¹]
143	2014.03.14	4:00	2.8	5	NULL	NULL	NULL	11	-1.11	55			NULL	NULL
144	2014.03.17	12:00	4.1	5	0	0	NULL	51	-0.76	24			NULL	NULL
145	2014.03.22	5:00	3.2	4	0	0	NULL	7	-1.09	3			NULL	NULL
146	2014.03.22	22:00	4	4	0	0	NULL	18	-0.74	8			NULL	NULL
147	2014.03.28	7:00	3.7	5	5	5	1.9	17	-1.16	3	2014.03.23	03:36:05	820	337
148	2014.03.29	19:00	2.5	3	0	0	NULL	33	-0.71	31			NULL	NULL
149	2014.04.02	18:00	2	4	0	0	NULL	1	-0.84	1			NULL	NULL
150	2014.04.04	20:00	2	5	5	5	0.8	8	-0.47	1	2014.03.28	23:48:07	514	253
151	2014.04.06	16:00	6.5	5	5	5	2.9	51	-0.9	45	2014.04.02	13:36:20	1471	422
152	2014.04.08	2:00	2.5	4	0	0	NULL	17	-0.92	11			NULL	NULL
153	2014.04.10	8:00	1.9	4	0	0	NULL	5	-0.76	1			NULL	NULL
154	2014.04.11	18:00	2.2	4	0	0	NULL	22	-0.74	4			NULL	NULL
155	2014.04.20	17:00	7.7	5	3	4	4.2	22	-1.23	3	2014.04.14	13:25:50	227	282
156	2014.04.22	2:00	1.9	4	4	4	1.7	6	-0.78	2	2014.04.18	13:25:51	1203	491
157	2014.04.28	6:00	2.6	4	0	0	NULL	11	-0.75	8			NULL	NULL
158	2014.05.06	6:00	3.9	4	0	0	NULL	29	-0.88	22			NULL	NULL
159	2014.05.11	22:00	1.5	4	0	0	NULL	4	-0.61	1			NULL	NULL
160	2014.05.15	17:00	1.6	4	0	0	NULL	16	-0.52	5			NULL	NULL
161	2014.05.17	6:00	3.1	5	0	0	NULL	22	-0.53	3			NULL	NULL
162	2014.05.23	13:00	4.7	5	3	3	2.3	32	-0.88	11			NULL	NULL
163	2014.05.27	9:00	1.6	2	3	0	NULL	16	-0.6	4			NULL	NULL
164	2014.05.29	13:00	2.6	3	0	0	NULL	8	-0.81	19			NULL	NULL
165	2014.06.01	13:00	2.3	4	2	0	NULL	8	-0.73	4			NULL	NULL
166	2014.06.09	18:00	3.1	4	4	3	4.5	23	-0.81	5	2014.06.04	12:48:05	467	332

Table 1 (Continued)

No.	Date	Time [UT]	AM [%]	q	q_S	q_E	A_E [%]	t_{min} [hrs]	DM_{in} [%]	tD_{Min} [hrs]	CME date	CME time [UT]	V_{CME} [km s^{-1}]	$V_{transit}$ [km s^{-1}]
167	2014.06.11	7:00	3.7	3	0	0	NULL	14	-0.99	11			NULL	NULL
168	2014.06.13	11:00	2	3	4	1	1.7	25	-0.81	2	2014.06.10	13:30:23	1469	598
169	2014.06.16	8:00	5.2	5	3	NULL	NULL	33	-0.85	4	2014.06.12	01:36:18	702	406
170	2014.06.17	11:00	5.6	5	3	NULL	NULL	26	-0.83	5	2014.06.12	04:36:07	609	329
171	2014.06.23	8:00	2.6	3	4	3	0.6	7	-1.18	3	2014.06.18	06:48:05	601	343
172	2014.06.25	15:00	3.7	4	4	4	0.5	29	-0.89	17	2014.06.19	17:00:05	416	293
173	2014.07.01	2:00	2.7	4	4	3	0.7	9	-1.26	1	2014.06.25	12:48:05	206	312
174	2014.07.03	21:00	2.7	4	4	1	NULL	5	-1.2	3	2014.06.30	17:12:05	542	548
175	2014.07.05	23:00	1.6	4	4	3	0.7	11	-0.85	1	2014.07.01	11:48:05	614	388
176	2014.07.06	22:00	1.6	5	3	0	NULL	17	-0.53	12	2014.07.01	03:48:05	181	301
177	2014.07.09	0:00	4.7	5	4	1	NULL	46	-0.8	22	2014.07.02	13:36:20	355	269
178	2014.07.13	16:00	1.5	4	4	3	1.2	15	-0.82	NULL	2014.07.08	16:36:05	773	348
179	2014.07.14	12:00	4.9	5	4	4	1.7	48	-1.04	46	2014.07.09	18:36:05	637	376
180	2014.07.17	10:00	1.6	4	0	0	NULL	9	-0.6	3			NULL	NULL
181	2014.07.23	19:00	2.6	5	3	0	NULL	4	-0.88	21	2014.07.20	03:12:09	417	473
182	2014.07.25	11:00	2.4	5	3	NULL	NULL	23	-0.79	17	2014.07.22	05:48:05	167	538
183	2014.08.01	9:00	7	5	4	1	NULL	29	-0.94	18	2014.07.28	14:30:35	1110	459
184	2014.08.06	18:00	2.5	4	3	1	NULL	12	-0.87	3	2014.08.01	18:36:05	789	347
185	2014.08.08	7:00	3.1	4	4	2	1.7	12	-0.9	7	2014.08.03	03:24:05	828	336
186	2014.08.14	6:00	2.2	2	0	0	NULL	8	-0.84	6			NULL	NULL
187	2014.08.24	7:00	2.2	3	0	0	NULL	12	-0.59	16			NULL	NULL
188	2014.08.26	7:00	2.8	4	4	0	NULL	30	-0.75	28	2014.08.20	15:48:05	283	307
189	2014.08.29	2:00	1.7	4	4	1	0.4	15	-0.89	1	2014.08.24	12:36:05	551	380
190	2014.08.31	11:00	2.4	2	0	0	NULL	132	-0.75	3			NULL	NULL

Table 1 (Continued)

No.	Date	Time [UT]	A_M [%]	q	q_S	q_E	A_E [%]	t_{min} [hrs]	DM_{in} [%]	tD_{Min} [hrs]	CME date	CME time [UT]	V_{CME} [$km\ s^{-1}$]	$V_{transit}$ [$km\ s^{-1}$]
191	2014.09.08	13:00	1.6	4	4	0	NULL	9	-0.8	7	2014.09.02	23:48:06	518	311
192	2014.09.09	18:00	2.9	4	4	0	NULL	6	-1.49	3	2014.09.05	07:12:05	740	388
193	2014.09.14	10:00	2	4	4	2	0.7	15	-0.8	10	2014.09.09	00:06:26	920	320
194	2014.09.16	11:00	1.5	4	0	0	NULL	8	-0.58	6			NULL	NULL
195	2014.09.18	20:00	4.4	5	0	0	NULL	33	-0.71	0			NULL	NULL
196	2014.09.21	5:00	5.8	4	0	0	NULL	86	-1	62			NULL	NULL
197	2014.09.29	5:00	2.6	4	3	0	NULL	14	-0.6	2	2014.09.24	21:30:06	1350	402
198	2014.09.30	6:00	4.2	5	5	1	NULL	16	-0.84	11	2014.09.26	04:28:16	1469	425
199	2014.10.03	3:00	1.9	5	0	0	NULL	8	-0.48	8			NULL	NULL
200	2014.10.05	9:00	2.1	4	4	0	NULL	10	-0.62	21			NULL	NULL
201	2014.10.09	8:00	2.1	3	3	1	NULL	9	-0.54	6	2014.10.02	04:24:05	875	242
202	2014.10.11	18:00	2.1	5	4	2	0.6	8	-0.99	6	2014.10.06	17:12:07	408	344
203	2014.10.16	18:00	4	5	4	1	NULL	16	-0.97	10	2014.10.13	00:12:05	521	463
204	2014.10.17	20:00	17.3	5	5	2	NULL	49	-1.44	6	2014.10.14	18:48:06	848	NULL
205	2014.11.03	6:00	2.9	3	3	0	NULL	20	-1.22	19	2014.10.28	20:24:05	467	320
206	2014.11.04	23:00	3.5	5	3	1	NULL	22	-0.67	NULL	2014.10.29	12:36:05	230	269
207	2014.11.08	10:00	5.4	5	3	2	NULL	22	-0.8	15	2014.11.03	12:00:05	447	NULL
208	2014.11.11	6:00	1.7	5	3	2	NULL	8	-0.53	5	2014.11.06	04:00:05	641	340
209	2014.11.13	12:00	1.8	4	3	2	5.1	12	-0.49	-3	2014.11.07	18:08:34	795	301
210	2014.11.15	10:00	5.2	5	0	0	NULL	29	-0.7	27			NULL	NULL
211	2014.11.18	8:00	4.9	5	0	0	NULL	30	-0.76	9			NULL	NULL
212	2014.11.22	18:00	3.3	5	2	0	NULL	23	-0.72	21			NULL	NULL
213	2014.11.25	6:00	4.5	5	0	0	NULL	56	-0.91	3			NULL	NULL
214	2014.11.28	13:00	4.2	5	3	1	NULL	35	-0.87	13	2014.11.23	16:12:05	601	355

Table 1 (Continued)

No.	Date	Time [UT]	AM [%]	q	qS	qE	A _E [%]	t _{min} [hrs]	DM _{in} [%]	tD _{min} [hrs]	CME date	CME time [UT]	V _{CME} [km s ⁻¹]	V _{transit} [km s ⁻¹]
215	2014.12.11	14:00	2	5	0	0	NULL	33	-0.76	2			NULL	NULL
216	2014.12.12	7:00	5.4	5	0	0	NULL	46	-0.73	40			NULL	NULL
217	2014.12.17	14:00	4.6	5	3	0	NULL	41	-0.63	24	2014.12.13	14:24:05	2222	435
218	2014.12.19	13:00	7.2	5	5	1	NULL	46	-0.89	44	2014.12.14	19:48:05	626	367
219	2014.12.27	14:00	2.1	3	4	0	NULL	16	-0.85	6			NULL	NULL
220	2015.01.13	5:00	5.2	5	0	0	NULL	33	-0.89	9			NULL	NULL
221	2015.01.18	1:00	5.5	4	0	0	NULL	32	-0.87	32			NULL	NULL
222	2015.01.29	16:00	3.1	5	0	0	NULL	2	-1.08	0			NULL	NULL
223	2015.02.01	13:00	3.4	4	3	1	NULL	11	-1.44	4			NULL	NULL
224	2015.02.07	0:00	4.2	4	0	0	NULL	27	-0.86	9			NULL	NULL
225	2015.02.08	22:00	2.8	5	0	0	NULL	16	-0.71	25			NULL	NULL
226	2015.02.10	7:00	3.1	5	0	0	NULL	26	-0.69	10			NULL	NULL
227	2015.02.12	3:00	3.4	5	3	1	NULL	29	-1.1	1			NULL	NULL
228	2015.02.13	20:00	4.5	5	4	2	1.2	24	-1.24	3	2015.02.09	23:24:05	1106	449
229	2015.02.16	22:00	3	4	4	1	NULL	36	-0.56	2			NULL	NULL
230	2015.02.21	11:00	2.3	4	3	1	NULL	33	-0.44	11			NULL	NULL
231	2015.02.27	9:00	2.1	3	2	0	NULL	14	-0.56	8			NULL	NULL
232	2015.03.03	12:00	13	5	4	0	NULL	45	-0.89	8	2015.02.28	21:36:05	999	666
233	2015.03.06	4:00	4.5	5	0	0	NULL	37	-0.92	13			NULL	NULL
234	2015.03.08	11:00	5.7	4	0	0	NULL	30	-0.91	8			NULL	NULL
235	2015.03.09	12:00	2.6	3	4	1	NULL	5	-0.93	3			NULL	NULL
236	2015.03.16	8:00	2.9	4	0	0	NULL	14	-0.83	12			NULL	NULL
237	2015.03.19	11:00	2.6	3	0	0	NULL	25	-0.92	20			NULL	NULL
238	2015.03.20	20:00	4.5	3	0	0	NULL	30	-0.87	8			NULL	NULL

Table 1 (Continued)

No.	Date	Time [UT]	AM [%]	q	qS	qE	A _E [%]	t _{min} [hrs]	DM _{in} [%]	tD _{Min} [hrs]	CME date	CME time [UT]	V _{CME} [kms ⁻¹]	V _{transit} [kms ⁻¹]
239	2015.03.24	23:00	3.7	5	0	0	NULL	19	-0.93	31			NULL	NULL
240	2015.03.28	10:00	8.7	4	0	0	NULL	61	-1.15	14			NULL	NULL
241	2015.04.01	2:00	2.6	4	3	0	2.7	9	-0.77	19	2015.03.27	13:36:05	440	383
242	2015.04.03	3:00	4.4	4	2	0	NULL	35	-1.04	3			NULL	NULL
243	2015.04.08	2:00	3.8	5	0	0	NULL	5	-0.58	32			NULL	NULL
244	2015.04.16	6:00	2.1	3	0	0	NULL	7	-0.99	14			NULL	NULL
245	2015.04.19	10:00	2	3	0	0	NULL	26	-0.66	22			NULL	NULL
246	2015.04.23	19:00	7.5	5	4	0	NULL	32	-1.06	3	2015.04.19	21:12:08	672	441
247	2015.04.26	13:00	5.4	4	0	0	NULL	45	-0.87	2			NULL	NULL
248	2015.05.02	15:00	3.9	5	4	0	NULL	9	-1.18	4	2015.04.25	14:48:05	675	247
249	2015.05.05	10:00	4	4	5	0	NULL	36	-0.85	20	2015.05.01	18:12:06	760	473
250	2015.05.11	7:00	4.1	4	0	0	NULL	16	-0.82	5			NULL	NULL
251	2015.05.12	13:00	2.6	3	0	0	NULL	21	-0.83	8			NULL	NULL
252	2015.05.14	9:00	2.8	3	0	0	NULL	24	-0.85	15			NULL	NULL
253	2015.05.17	11:32	2	3	0	0	NULL	26	-0.62	3			NULL	NULL
254	2015.05.21	15:00	3.4	2	0	0	NULL	43	-1.09	50			NULL	NULL
255	2015.05.25	5:00	3.3	4	3	1	NULL	18	-0.83	7	2015.05.21	22:24:06	978	529
256	2015.05.28	6:00	1.9	4	0	0	NULL	17	-0.92	9			NULL	NULL
257	2015.06.12	8:00	4.2	4	0	NULL	NULL	31	-0.91	21			NULL	NULL
258	2015.06.15	6:00	1.6	3	0	NULL	NULL	28	-0.85	26			NULL	NULL
259	2015.06.21	6:00	1.9	4	0	0	NULL	6	-0.94	4			NULL	NULL
260	2015.06.22	11:00	8	4	3	0	NULL	25	-0.85	48	2015.06.15	13:57:56	146	251
261	2015.06.24	6:00	2	3	0	0	NULL	10	-0.89	5			NULL	NULL
262	2015.06.28	5:00	2.8	5	0	0	NULL	10	-1.14	3			NULL	NULL

Table 1 (Continued)

No.	Date	Time [UT]	A_M [%]	q	q_S	q_E	A_E [%]	t_{min} [hrs]	DM_{in} [%]	tD_{Min} [hrs]	CME date	CME time [UT]	V_{CME} [km s^{-1}]	$V_{transit}$ [km s^{-1}]
263	2015.06.30	15:00	6.4	4	0	0	NULL	27	-0.83	12			NULL	NULL
264	2015.07.02	18:00	2.7	4	0	0	NULL	14	-0.77	NULL			NULL	NULL
265	2015.07.04	14:00	1.3	3	4	0	NULL	5	-0.51	1	2015.07.01	14:36:04	1435	582
266	2015.07.08	0:00	2.9	5	0	0	NULL	26	-0.82	2			NULL	NULL
267	2015.07.10	1:00	1.8	5	0	0	NULL	17	-0.44	1			NULL	NULL
268	2015.07.12	16:00	3	4	0	0	NULL	12	-1.04	1			NULL	NULL
269	2015.07.14	19:00	2.4	4	0	0	NULL	6	-1.09	14			NULL	NULL
270	2015.07.24	5:00	2.5	5	0	0	NULL	8	-0.69	6			NULL	NULL
271	2015.07.27	3:00	2.6	4	3	0	NULL	8	-0.78	8			NULL	NULL
272	2015.07.29	4:00	1.7	5	0	0	NULL	17	-0.65	8			NULL	NULL
273	2015.07.31	17:00	1.6	4	3	0	NULL	6	-0.81	20			NULL	NULL
274	2015.08.01	20:00	2.7	5	4	0	NULL	13	-0.57	10			NULL	NULL
275	2015.08.06	8:00	2.9	3	0	0	NULL	8	-0.83	3			NULL	NULL
276	2015.08.12	7:00	2.8	5	0	0	NULL	6	-0.63	9			NULL	NULL
277	2015.08.17	5:00	2.2	4	0	0	NULL	10	-0.74	24			NULL	NULL
278	2015.08.21	3:00	4.6	5	0	0	NULL	73	-1.03	18			NULL	NULL
279	2015.08.24	8:00	2.3	4	0	0	NULL	8	-0.89	3			NULL	NULL
280	2015.08.26	2:00	2.1	5	4	0	NULL	9	-1.21	1			NULL	NULL
281	2015.08.29	0:00	3.4	4	0	0	NULL	20	-0.71	7			NULL	NULL
282	2015.09.02	14:00	3.9	5	3	0	NULL	8	-0.84	6			NULL	NULL
283	2015.09.06	3:00	2.4	4	0	0	NULL	6	-0.47	4			NULL	NULL
284	2015.09.09	18:00	4.1	4	0	0	NULL	59	-0.98	0			NULL	NULL
285	2015.09.18	16:00	3.6	4	0	0	NULL	25	-0.59	3			NULL	NULL
286	2015.09.22	6:00	2.3	4	0	0	NULL	4	-0.68	4			NULL	NULL

Table 1 (Continued)

No.	Date	Time [UT]	A_M [%]	q	q_S	q_E	A_E [%]	t_{min} [hrs]	DM_{in} [%]	tD_{min} [hrs]	CME date	CME time [UT]	V_{CME} [$km\ s^{-1}$]	$V_{transit}$ [$km\ s^{-1}$]
287	2015.09.25	5:00	2.5	3	0	0	NULL	26	-0.67	18			NULL	NULL
288	2015.09.28	23:00	2	4	0	0	NULL	8	-0.72	1			NULL	NULL
289	2015.10.03	3:00	1.9	3	0	0	NULL	31	-0.54	36			NULL	NULL
290	2015.10.04	22:00	3	2	0	3	NULL	88	-1	88	2015.09.30	10:00:04	602	386
291	2015.10.09	17:00	3.5	2	4	1	NULL	23	-0.57	22			NULL	NULL
292	2015.10.12	5:00	2.1	5	4	0	NULL	28	-0.8	11	2015.10.07	07:36:04	900	354
293	2015.10.14	10:00	2.7	4	0	0	NULL	24	-0.88	24			NULL	NULL
294	2015.10.16	7:00	1.8	3	0	0	NULL	7	-0.7	3			NULL	NULL
295	2015.10.18	3:00	5.4	4	0	0	NULL	50	-0.94	3			NULL	NULL
296	2015.10.23	10:00	2.7	3	0	0	NULL	22	-0.57	48			NULL	NULL
297	2015.10.26	2:00	3	3	0	0	NULL	32	-0.94	3			NULL	NULL
298	2015.11.03	12:00	1.8	2	0	0	NULL	11	-0.75	10			NULL	NULL
299	2015.11.06	22:00	2.1	5	0	0	NULL	22	-0.62	1			NULL	NULL
300	2015.11.08	1:00	4.2	5	4	1	NULL	21	-0.76	21	2015.11.02	20:24:04	867	335
301	2015.11.09	17:00	1.4	5	0	0	NULL	2	-0.63	8			NULL	NULL
302	2015.11.13	7:00	3.5	5	0	0	NULL	39	-0.67	37			NULL	NULL
303	2015.11.16	1:00	3.2	5	0	0	NULL	15	-0.96	13			NULL	NULL
304	2015.11.17	17:00	2.2	5	3	2	1.3	20	-0.8	16	2015.11.11	15:24:04	629	285
305	2015.11.19	22:00	4	5	0	0	NULL	25	-0.73	6			NULL	NULL
306	2015.11.21	4:00	3.9	5	0	0	NULL	29	-0.63	27			NULL	NULL
307	2015.11.24	5:00	3	4	0	0	NULL	25	-0.49	9			NULL	NULL
308	2015.11.28	1:00	2.3	4	0	0	NULL	19	-1.19	4			NULL	NULL
309	2015.12.01	16:00	2.3	4	0	0	NULL	24	-0.65	2			NULL	NULL
310	2015.12.07	9:00	2.8	3	0	0	NULL	25	-0.86	23			NULL	NULL

Table 1 (Continued)

No.	Date	Time [UT]	AM [%]	q	qS	qE	A _E [%]	t _{min} [hrs]	DM _{in} [%]	tD _{min} [hrs]	CME date	CME time [UT]	V _{CME} [km s ⁻¹]	V _{transit} [km s ⁻¹]
311	2015.12.14	18:00	4.4	5	0	0	NULL	22	-0.82	19			NULL	NULL
312	2015.12.15	21:00	6.9	5	0	0	NULL	34	-0.63	14			NULL	NULL
313	2015.12.19	6:00	3.7	4	0	0	NULL	66	-0.72	26			NULL	NULL
314	2015.12.22	17:00	1.8	4	0	0	NULL	19	-0.59	17			NULL	NULL
315	2015.12.30	21:00	1.6	4	0	0	NULL	6	-0.63	4			NULL	NULL
316	2016.01.02	16:00	3.4	5	0	0	NULL	25	-0.79	4			NULL	NULL
317	2016.01.04	7:00	6.1	5	4	1	NULL	50	-0.74	31	2016.01.01	23:24:04	1730	747
318	2016.01.11	22:00	3.3	3	0	0	NULL	32	-1.24	25			NULL	NULL
319	2016.01.15	0:00	2.4	3	0	0	NULL	18	-0.65	11			NULL	NULL
320	2016.01.17	23:00	2.3	3	0	0	NULL	11	-0.52	8			NULL	NULL
321	2016.01.21	8:00	1.9	3	4	3	2.1	24	-0.55	40	2016.01.14	23:24:05	191	272
322	2016.01.25	18:00	3.2	4	0	0	NULL	26	-0.86	16			NULL	NULL
323	2016.01.27	22:00	2.7	3	0	0	NULL	23	-0.61	12			NULL	NULL
324	2016.02.01	8:00	3.9	4	0	0	NULL	25	-0.79	3			NULL	NULL
325	2016.02.04	1:00	6	4	4	1	NULL	23	-1.09	7			NULL	NULL
326	2016.02.05	22:00	2.5	3	0	0	NULL	11	-0.77	3			NULL	NULL
327	2016.02.08	15:00	3.9	3	0	0	NULL	13	-0.83	23			NULL	NULL
328	2016.02.09	8:00	3.9	3	0	0	NULL	9	-0.86	6			NULL	NULL
329	2016.02.11	20:00	2	3	3	2	0.8	18	-0.65	1	2016.02.05	17:24:04	250	283
330	2016.02.13	11:00	1.5	3	2	2	1.4	13	-0.58	-3	2016.02.07	03:36:04	232	274
331	2016.02.14	14:00	3.1	3	3	2	NULL	24	-0.65	2	2016.02.09	06:00:04	581	325
332	2016.02.17	18:00	2.1	4	5	2	1	23	-0.57	1	2016.02.11	21:17:32	719	295
333	2016.02.22	3:00	2.5	3	0	0	NULL	33	-0.59	19			NULL	NULL
334	2016.03.01	4:00	4.6	5	0	0	NULL	52	-0.71	50			NULL	NULL

Table 1 (Continued)

No.	Date	Time [UT]	AM [%]	q	qS	qE	A _E [%]	t _{min} [hrs]	DM _{in} [%]	tD _{min} [hrs]	CME date	CME time [UT]	V _{CME} [km s ⁻¹]	V _{transit} [km s ⁻¹]
335	2016.03.06	0:00	3.5	3	0	0	NULL	12	-0.92	3			NULL	NULL
336	2016.03.07	8:00	2.9	3	0	0	NULL	8	-0.93	6			NULL	NULL
337	2016.03.10	23:00	5	5	0	0	NULL	34	-0.78	32			NULL	NULL
338	2016.03.16	8:00	3	4	0	0	NULL	26	-0.77	35			NULL	NULL
339	2016.03.19	7:00	2.9	4	0	0	NULL	25	-0.89	23			NULL	NULL
340	2016.03.21	6:00	1.7	4	4	1	NULL	23	-0.82	30	2016.03.16	07:00:04	592	349
341	2016.03.26	21:00	2	4	0	0	NULL	25	-0.64	15			NULL	NULL
342	2016.03.27	18:00	5.6	5	0	0	NULL	29	-1.12	9			NULL	NULL
343	2016.04.02	4:00	1.8	4	0	0	NULL	13	-0.62	40			NULL	NULL
344	2016.04.06	4:00	2.4	4	0	0	NULL	7	-0.61	1			NULL	NULL
345	2016.04.13	2:00	3.3	5	4	3	1.4	22	-0.46	4	2016.04.06	15:12:08	353	268
346	2016.04.14	23:00	4	5	0	0	NULL	41	-0.88	19			NULL	NULL
347	2016.04.16	9:00	2.9	5	3	3	2.2	12	-0.75	11	2016.04.10	11:12:05	543	293
348	2016.04.18	9:00	1.2	4	0	0	NULL	6	-0.61	4			NULL	NULL
349	2016.04.21	8:00	1.1	3	0	0	NULL	8	-0.59	1			NULL	NULL
350	2016.04.22	10:00	2	5	4	1	NULL	18	-0.63	-3	2016.04.18	00:48:04	1084	395
351	2016.04.24	11:00	4.3	5	0	0	NULL	24	-0.77	35			NULL	NULL
352	2016.04.30	22:00	2.1	3	0	0	NULL	13	-0.56	0			NULL	NULL
353	2016.05.04	3:00	3.2	5	3	2	NULL	23	-0.77	17			NULL	NULL
354	2016.05.09	17:00	5.2	4	0	0	NULL	23	-0.91	5			NULL	NULL
355	2016.05.15	23:00	2.1	5	4	4	1.2	19	-0.55	10	2016.05.09	20:12:22	347	283
356	2016.05.18	0:00	2.2	5	0	0	NULL	25	-0.51	22			NULL	NULL
357	2016.05.19	4:00	3.9	5	0	0	NULL	34	-0.74	20			NULL	NULL
358	2016.05.25	7:00	2.4	5	0	0	NULL	14	-0.73	10			NULL	NULL

Table 1 (Continued)

No.	Date	Time [UT]	AM [%]	q	qS	qE	A _E [%]	t _{min} [hrs]	DM _{in} [%]	tD _{min} [hrs]	CME date	CME time [UT]	V _{CME} [km s ⁻¹]	V _{transit} [km s ⁻¹]
359	2016.05.31	6:00	2.5	5	0	0	NULL	23	-0.48	1			NULL	NULL
360	2016.06.03	2:00	1.6	3	0	0	NULL	8	-0.57	8			NULL	NULL
361	2016.06.06	22:00	3.3	5	0	0	NULL	11	-0.61	11			NULL	NULL
362	2016.06.07	3:00	2.8	4	0	0	NULL	6	-0.61	6			NULL	NULL
363	2016.06.12	14:00	4	5	0	0	NULL	46	-0.75	46			NULL	NULL
364	2016.06.15	5:00	5.6	5	0	0	NULL	29	-1.02	7			NULL	NULL
365	2016.06.16	19:00	3.3	4	0	0	NULL	35	-0.7	3			NULL	NULL
366	2016.06.18	18:00	2.5	3	3	4	0.9	6	-0.58	35	2016.06.14	13:25:44	460	413
367	2016.06.20	17:00	3.4	4	0	0	NULL	11	-0.56	2			NULL	NULL
368	2016.06.23	8:00	2.8	4	4	2	NULL	52	-0.68	44	2016.06.16	07:48:05	314	247
369	2016.06.24	23:00	3.1	5	0	0	NULL	13	-0.88	56			NULL	NULL
370	2016.06.27	6:00	2.3	2	0	0	NULL	11	-0.88	1			NULL	NULL
371	2016.07.02	20:00	2.9	3	0	0	NULL	20	-0.6	18			NULL	NULL
372	2016.07.07	23:00	4.4	2	0	0	NULL	48	-0.79	21			NULL	NULL
373	2016.07.12	1:00	4.4	3	0	0	NULL	56	-0.94	1			NULL	NULL
374	2016.07.19	21:00	3	5	0	0	NULL	52	-0.9	30			NULL	NULL
375	2016.07.24	22:00	3.6	3	3	3	0.3	8	-0.86	23			NULL	NULL
376	2016.07.28	23:00	2.9	5	0	0	NULL	8	-0.7	33			NULL	NULL
377	2016.08.02	2:00	3.6	4	0	0	NULL	24	-0.56	13			NULL	NULL
378	2016.08.04	9:00	5	4	4	3	3	35	-0.62	22			NULL	NULL
379	2016.08.12	0:00	2.3	4	0	0	NULL	13	-0.6	36			NULL	NULL
380	2016.08.15	7:00	2.7	4	4	1	NULL	20	-0.54	28			NULL	NULL
381	2016.08.18	15:00	2.3	5	0	0	NULL	10	-0.58	8			NULL	NULL
382	2016.08.21	22:00	1.6	3	0	0	NULL	16	-0.97	1			NULL	NULL

Table 1 (Continued)

No.	Date	Time [UT]	AM [%]	<i>q</i>	<i>q_S</i>	<i>q_E</i>	<i>A_E</i> [%]	<i>t_{min}</i> [hrs]	<i>DM_{in}</i> [%]	<i>tD_{Min}</i> [hrs]	CME date	CME time [UT]	<i>V_{CME}</i> [km s ⁻¹]	<i>V_{transit}</i> [km s ⁻¹]
383	2016.08.23	15:00	2.2	5	0	0	NULL	9	-0.57	22			NULL	NULL
384	2016.08.26	0:00	3.3	5	0	0	NULL	9	-0.51	3			NULL	NULL
385	2016.08.28	20:00	1.9	4	0	0	NULL	18	-0.69	4			NULL	NULL
386	2016.08.29	19:00	4.5	5	0	0	NULL	41	-0.8	41			NULL	NULL
387	2016.09.01	4:00	6.2	5	0	0	NULL	39	-0.82	23			NULL	NULL
388	2016.09.06	11:00	2	5	0	0	NULL	8	-0.53	29			NULL	NULL
389	2016.09.07	14:00	2.5	4	0	0	NULL	23	-0.59	35			NULL	NULL
390	2016.09.08	21:00	7.3	5	0	0	NULL	19	-1.72	6			NULL	NULL
391	2016.09.17	12:00	3.6	3	0	0	NULL	23	-0.63	4			NULL	NULL
392	2016.09.23	8:00	2.9	3	0	0	NULL	10	-0.8	9			NULL	NULL
393	2016.09.27	19:00	2.7	3	0	0	NULL	6	-0.73	-4			NULL	NULL
394	2016.09.30	5:00	1.9	3	0	0	NULL	37	-0.51	2			NULL	NULL
395	2016.10.05	22:00	2.5	4	0	0	NULL	10	-0.48	32			NULL	NULL
396	2016.10.09	6:00	4.4	4	0	0	NULL	34	-0.86	21			NULL	NULL
397	2016.10.13	6:00	2	5	0	0	NULL	6	-0.58	2			NULL	NULL
398	2016.10.14	9:00	4.3	5	4	3	1.8	22	-0.73	20			NULL	NULL
399	2016.10.15	22:00	3.1	4	0	0	NULL	6	-0.8	4			NULL	NULL
400	2016.10.18	4:00	2.8	4	0	0	NULL	4	-0.36	2			NULL	NULL
401	2016.10.19	7:00	2.4	4	3	0	NULL	17	-0.4	12			NULL	NULL
402	2016.10.20	9:00	4.3	4	0	0	NULL	89	-0.73	55			NULL	NULL
403	2016.10.25	16:00	2.5	3	0	0	NULL	14	-0.62	23			NULL	NULL
404	2016.10.29	9:00	3.2	3	0	0	NULL	5	-0.79	24			NULL	NULL
405	2016.10.30	22:00	3.8	3	0	0	NULL	24	-0.5	22			NULL	NULL
406	2016.11.03	21:00	2	4	0	0	NULL	10	-0.5	14			NULL	NULL

Table 1 (Continued)

No.	Date	Time [UT]	AM [%]	q	q_S	q_E	A_E [%]	t_{min} [hrs]	DM_{in} [%]	tD_{Min} [hrs]	CME date	CME time [UT]	V_{CME} [km s^{-1}]	$V_{transit}$ [km s^{-1}]
407	2016.11.05	15:00	3	5	0	0	NULL	6	-0.55	4			NULL	NULL
408	2016.11.06	23:00	3.1	4	0	0	NULL	36	-0.61	23			NULL	NULL
409	2016.11.08	22:00	2.9	5	0	0	NULL	10	-0.57	5			NULL	NULL
410	2016.11.10	8:00	1.4	3	0	0	NULL	28	-0.55	26			NULL	NULL
411	2016.11.12	4:00	2.7	3	3	2	NULL	2	-0.49	2			NULL	NULL
412	2016.11.17	18:00	6	5	0	0	NULL	65	-0.68	18			NULL	NULL
413	2016.11.22	11:00	2.9	3	0	0	NULL	11	-0.71	3			NULL	NULL
414	2016.11.25	6:00	2	3	0	0	NULL	4	-0.71	48			NULL	NULL
415	2016.11.28	19:00	2.9	4	0	0	NULL	3	-0.72	15			NULL	NULL
416	2016.12.01	12:00	2.3	3	0	0	NULL	18	-0.92	55			NULL	NULL
417	2016.12.05	3:00	1.8	3	0	0	NULL	34	-0.61	14			NULL	NULL
418	2016.12.13	3:00	2	4	0	0	NULL	11	-0.8	23			NULL	NULL
419	2016.12.14	18:00	5.3	5	0	0	NULL	34	-0.68	6			NULL	NULL
420	2016.12.17	9:00	2.1	4	0	0	NULL	8	-0.74	27			NULL	NULL
421	2016.12.19	5:00	2.3	3	0	0	NULL	20	-0.92	18			NULL	NULL
422	2016.12.20	21:00	2.7	4	0	0	NULL	50	-0.76	30			NULL	NULL
423	2016.12.26	22:00	2.5	4	0	0	NULL	18	-0.69	34			NULL	NULL
424	2016.12.28	6:00	1.8	2	0	0	NULL	0	0	0			NULL	NULL

References

- Abunin, A., Abunina, M., Belov, A., Eroshenko, E., Oleneva, V., Yanke, V.: 2012, Forbush effects with a sudden and gradual onset. *Geomagn. Aeron.* **52**(3), 292. DOI.
- Abunin, A., Abunina, M., Belov, A., Eroshenko, E., Oleneva, V., Yanke, V.: 2013, Forbush-decreases in 19th solar cycle. *J. Phys. Conf. Ser.* **409**, 012165. DOI.
- Abunina, M., Abunin, A., Belov, A., Eroshenko, E., Oleneva, V., Yanke, V.: 2013a, Long-period variations in the amplitude-phase interrelation of the first cosmic ray anisotropy harmonic. *Geomagn. Aeron.* **53**(5), 561. DOI.
- Abunina, M., Abunin, A., Belov, A., Eroshenko, E., Asipenka, A., Oleneva, V., Yanke, V.: 2013b, Relationship between Forbush effect parameters and the heliolongitude of solar sources. *Geomagn. Aeron.* **53**(1), 10. DOI.
- Abunina, M., Abunin, A., Belov, A., Eroshenko, E., Oleneva, V., Yanke, V.: 2015, Phase distribution of the first harmonic of the cosmic ray anisotropy during the initial phase of Forbush effects. *J. Phys. Conf. Ser.* **632**, 012044. DOI.
- Arge, C., Pizzo, V.: 2000, Improvement in the prediction of solar wind conditions using near-real time solar magnetic field updates. *J. Geophys. Res.* **105**(A5), 10465. DOI.
- Arge, C., Luhmann, J., Odstrcil, D., Schrijver, C., Li, Y.: 2004, Stream structure and coronal sources of the solar wind during the May 12th, 1997 CME. *J. Atmos. Solar-Terr. Phys.* **66**(15), 1295. DOI.
- Asipenka, A., Belov, A., Eroshenko, E., Klepach, E., Oleneva, V., Yanke, V.: 2009, Interactive database of cosmic ray anisotropy (DB-A10). *Adv. Space Res.* **43**(4), 708. DOI.
- Belov, A.: 1987, The first harmonic of cosmic ray anisotropy in the convection-diffusion model. In: *International Cosmic Ray Conference* **4**, 119.
- Belov, A.V.: 2009, Forbush effects and their connection with solar, interplanetary and geomagnetic phenomena. In: Gopalswamy, N., Webb, D.F. (eds.) *Universal Heliophysical Processes, IAU Symposium* **257**, 439. DOI. ADS.
- Belov, A., Eroshenko, E., Oleneva, V., Struminsky, A., Yanke, V.: 2001, What determines the magnitude of Forbush decreases? *Adv. Space Res.* **27**(3), 625. DOI.
- Belov, A., Abunin, A., Abunina, M., Eroshenko, E., Oleneva, V., Yanke, V., Papaioannou, A., Mavromichalaki, H.: 2015, Galactic cosmic ray density variations in magnetic clouds. *Solar Phys.* **290**(5), 1429. DOI.
- Belov, A., Eroshenko, E., Yanke, V., Oleneva, V., Abunin, A., Abunina, M., Papaioannou, A., Mavromichalaki, H.: 2018, The global survey method applied to ground-level cosmic ray measurements. *Solar Phys.* **293**(4), 68. DOI.
- Brueckner, G., Howard, R., Koomen, M., Korendyke, C., Michels, D., Moses, J., Socker, D., Dere, K., Lamy, P., Llebaria, A., et al.: 1995, The Large Angle Spectroscopic Coronagraph (LASCO). *Solar Phys.* **162**(1–2), 357. DOI.
- Burlaga, L., Plunkett, S., St. Cyr, O.: 2002, Successive CMEs and complex ejecta. *J. Geophys. Res.* **107**(A10), 1266. DOI.
- Burlaga, L., Berdichevsky, D., Gopalswamy, N., Lepping, R., Zurbuchen, T.: 2003, Merged interaction regions at 1 AU. *J. Geophys. Res.* **108**(A12), 1425. DOI.
- Cane, H.V.: 2000, Coronal mass ejections and Forbush decreases. *Space Sci. Rev.* **93**(1), 55. DOI.
- Cane, H., Richardson, I., Wibberenz, G.: 1995, The response of energetic particles to the presence of ejecta material. In: *International Cosmic Ray Conference* **4**, 377.
- Clauset, A., Shalizi, C.R., Newman, M.E.: 2009, Power-law distributions in empirical data. *SIAM Rev.* **51**(4), 661. DOI.
- Clem, J.M., Dorman, L.I.: 2000, Neutron monitor response functions. *Space Sci. Rev.* **93**(1), 335. DOI.
- Domingo, V., Fleck, B., Poland, A.: 1995, SOHO: The Solar and Heliospheric Observatory. *Space Sci. Rev.* **72**(1–2), 81. DOI.
- Dumbović, M., Heber, B., Vršnak, B., Temmer, M., Kirin, A.: 2018, An analytical diffusion–expansion model for Forbush decreases caused by flux ropes. *Astrophys. J.* **860**(1), 71. DOI.
- Ehresmann, B., Zeitlin, C., Hassler, D.M., Wimmer-Schweingruber, R.F., Böhm, E., Böttcher, S., Brinza, D.E., Burmeister, S., Guo, J., Köhler, J., et al.: 2014, Charged particle spectra obtained with the Mars Science Laboratory Radiation Assessment Detector (MSL/RAD) on the surface of Mars. *J. Geophys. Res.* **119**(3), 468. DOI.
- Forbush, S.: 1938, On cosmic-ray effects associated with magnetic storms. *J. Geophys. Res.* **43**(3), 203. DOI.
- Freiherr von Forstner, J.L., Guo, J., Wimmer-Schweingruber, R.F., Hassler, D.M., Temmer, M., Dumbović, M., Jian, L.K., Appel, J.K., Čalogović, J., Ehresmann, B., et al.: 2018, Using Forbush decreases to derive the transit time of ICMEs propagating from 1 AU to Mars. *J. Geophys. Res.* **123**(1), 39. DOI.
- Gopalswamy, N., Yashiro, S., Michalek, G., Stenborg, G., Vourlidas, A., Freeland, S., Howard, R.: 2009, The SOHO/LASCO CME Catalog. *Earth Moon Planets* **104**, 295. DOI. ADS.

- Grotzinger, J.P., Crisp, J., Vasavada, A.R., Anderson, R.C., Baker, C.J., Barry, R., Blake, D.F., Conrad, P., Edgett, K.S., Ferdowski, B., *et al.*: 2012, Mars Science Laboratory mission and science investigation. *Space Sci. Rev.* **170**(1–4), 5. DOI.
- Guo, J., Zeitlin, C., Wimmer-Schweingruber, R.F., Rafkin, S., Hassler, D.M., Posner, A., Heber, B., Köhler, J., Ehresmann, B., Appel, J.K., *et al.*: 2015, Modeling the variations of dose rate measured by RAD during the first MSL Martian year: 2012–2014. *Astrophys. J.* **810**(1), 24. DOI.
- Guo, J., Slaba, T.C., Zeitlin, C., Wimmer-Schweingruber, R.F., Badavi, F.F., Böhm, E., Böttcher, S., Brinza, D.E., Ehresmann, B., Hassler, D.M., *et al.*: 2017, Dependence of the Martian radiation environment on atmospheric depth: modeling and measurement. *J. Geophys. Res.* **122**(2), 329. DOI.
- Guo, J., Lillis, R., Wimmer-Schweingruber, R.F., Zeitlin, C., Simonson, P., Rahmati, A., Posner, A., Papaioannou, A., Lundt, N., Lee, C.O., *et al.*: 2018, Measurements of Forbush decreases at Mars: both by MSL on ground and by MAVEN in orbit. *Astron. Astrophys.* **611**, A79.
- Guo, J., Wimmer-Schweingruber, R.F., Grande, M., Lee-Payne, Z.H., Matthäi, D.: 2019, Ready functions for calculating the martian radiation environment. *J. Space Weather Space Clim.* **9**, A7. DOI.
- Hassler, D., Zeitlin, C., Wimmer-Schweingruber, R., Böttcher, S., Martin, C., Andrews, J., Böhm, E., Brinza, D., Bullock, M., Burmeister, S., *et al.*: 2012, The Radiation Assessment Detector (RAD) investigation. *Space Sci. Rev.* **170**(1–4), 503. DOI.
- Hassler, D.M., Zeitlin, C., Wimmer-Schweingruber, R.F., Ehresmann, B., Rafkin, S., Eigenbrode, J.L., Brinza, D.E., Weigle, G., Böttcher, S., Böhm, E., *et al.*: 2014, Mars' surface radiation environment measured with the Mars Science Laboratory's Curiosity rover. *Science* **343**(6169), 1244797. DOI.
- Heber, B., Wallmann, C., Galsdorf, D., Herbst, K., Kühl, P., Dumbović, M., Vršnak, B., Veronig, A., Temmer, M., Möstl, C., *et al.*: 2015, Forbush decreases associated to stealth coronal mass ejections. *Cent. Eur. Astrophys. Bull.* **39**, 75.
- Iucci, N., Parisi, M., Storini, M., Villoresi, G.: 1979, High-speed solar-wind streams and galactic cosmic-ray modulation. *Nuovo Cimento C* **2**(4), 421. DOI.
- Jordan, A., Spence, H.E., Blake, J., Mulligan, T., Shaul, D., Galametz, M.: 2009, Multipoint, high time resolution galactic cosmic ray observations associated with two interplanetary coronal mass ejections. *J. Geophys. Res.* **114**(A7), A07107. DOI.
- Jordan, A., Spence, H.E., Blake, J., Shaul, D.: 2011, Revisiting two-step Forbush decreases. *J. Geophys. Res.* **116**(A11), A11103. DOI.
- Klyueva, A., Belov, A., Eroshenko, E.: 2017, Specific features of the rigidity spectrum of Forbush effects. *Geomagn. Aeron.* **57**(2), 177. DOI.
- Köhler, J., Zeitlin, C., Ehresmann, B., Wimmer-Schweingruber, R.F., Hassler, D.M., Reitz, G., Brinza, D., Weigle, G., Appel, J., Böttcher, S., *et al.*: 2014, Measurements of the neutron spectrum on the martian surface with MSL/RAD. *J. Geophys. Res.* **119**(3), 594.
- Kryakunova, O., Tsepakina, I., Nikolayevskiy, N., Malimbayev, A., Belov, A., Abunin, A., Abunina, M., Eroshenko, E., Oleneva, V., Yanke, V.: 2013, Influence of high-speed streams from coronal holes on cosmic ray intensity in 2007. *J. Phys. Conf. Ser.* **409**, 012181. DOI.
- Kryakunova, O., Belov, A., Abunin, A., Abunina, M., Eroshenko, E., Malimbayev, A., Tsepakina, I., Yanke, V.: 2015, Recurrent and sporadic Forbush-effects in deep solar minimum. *J. Phys. Conf. Ser.* **632**, 012062. DOI.
- Liu, Y.D., Luhmann, J.G., Möstl, C., Martinez-Oliveros, J.C., Bale, S.D., Lin, R.P., Harrison, R.A., Temmer, M., Webb, D.F., Odstrcil, D.: 2012, Interaction between coronal mass ejections viewed in coordinated imaging and in situ observations. *Astrophys. J.* **746**(2), L15. DOI.
- Lockwood, J.A.: 1971, Forbush decreases in the cosmic radiation. *Space Sci. Rev.* **12**(5), 658. DOI.
- Lugaz, N., Farrugia, C.: 2014, A new class of complex ejecta resulting from the interaction of two CMEs and its expected geoeffectiveness. *Geophys. Res. Lett.* **41**(3), 769. DOI.
- McDonald, F., Trainor, J., Webber, W.: 1981, Pioneer and Voyager observations of Forbush decreases between 6 and 24 AU. In: *International Cosmic Ray Conference* **10**, 147.
- Möstl, C., Rollett, T., Frahm, R.A., Liu, Y.D., Long, D.M., Colaninno, R.C., Reiss, M.A., Temmer, M., Farrugia, C.J., Posner, A., *et al.*: 2015, Strong coronal channelling and interplanetary evolution of a solar storm up to Earth and Mars. *Nat. Commun.* **6**, 7135. DOI.
- Newman, M.E.: 2005, Power laws, Pareto distributions and Zipf's law. *Contemp. Phys.* **46**(5), 323. DOI.
- Papaioannou, A., Mavromichalaki, H., Eroshenko, E., Belov, A., Oleneva, V.: 2005, The burst of solar and geomagnetic activity in August–September. *Ann. Geophys.* **27**, 1019. DOI. 2009a.
- Papaioannou, A., Belov, A., Mavromichalaki, H., Eroshenko, E., Oleneva, V.: 2009b, The unusual cosmic ray variations in July 2005 resulted from western and behind the limb solar activity. *Adv. Space Res.* **43**, 582. DOI.
- Papaioannou, A., Malandraki, O., Belov, A., Skoug, R., Mavromichalaki, H., Eroshenko, E., Abunin, A., Lepri, S.: 2010, On the analysis of the complex Forbush decreases of January 2005. *Solar Phys.* **266**(1), 181. DOI.

- Papaioannou, A., Souvatzoglou, G., Paschalis, P., Gerontidou, M., Mavromichalaki, H.: 2014, The first ground-level enhancement of solar cycle 24 on 17 May 2012 and its real-time detection. *Solar Phys.* **289**(1), 423. DOI.
- Parker, E.: 1965, Dynamical theory of the solar wind. *Space Sci. Rev.* **4**(5–6), 666. DOI.
- Rafkin, S.C., Zeitlin, C., Ehresmann, B., Hassler, D., Guo, J., Köhler, J., Wimmer-Schweingruber, R., Gomez-Elvira, J., Harri, A.-M., Kahanpää, H., et al.: 2014, Diurnal variations of energetic particle radiation at the surface of Mars as observed by the Mars Science Laboratory Radiation Assessment Detector. *J. Geophys. Res.* **119**(6), 1345. DOI.
- Richardson, I., Cane, H.: 2011, Galactic cosmic ray intensity response to interplanetary coronal mass ejections/magnetic clouds in 1995–2009. *Solar Phys.* **270**(2), 609. DOI.
- Roussos, E., Jackman, C., Thomsen, M., Kurth, W., Badman, S., Paranicas, C., Kollmann, P., Krupp, N., Bučík, R., Mitchell, D., et al.: 2017, Solar energetic particles (SEP) and galactic cosmic rays (GCR) as tracers of solar wind conditions near Saturn: event lists and applications. *Icarus* **300**, 47. DOI.
- Shea, M., Smart, D.: 2012, Space weather and the ground-level solar proton events of the 23rd solar cycle. *Space Sci. Rev.* **171**(1–4), 161. DOI.
- Temmer, M., Vršnak, B., Rollett, T., Bein, B., de Koning, C.A., Liu, Y., Bosman, E., Davies, J.A., Möstl, C., Žic, T., et al.: 2012, Characteristics of kinematics of a coronal mass ejection during the 2010 August 1 CME–CME interaction event. *Astrophys. J.* **749**(1), 57. DOI.
- Van Allen, J.A., Fillius, R.W.: 1992, Propagation of a large Forbush decrease in cosmic-ray intensity past the Earth, Pioneer 11 at 34 AU, and Pioneer 10 at 53 AU. *Geophys. Res. Lett.* **19**(14), 1423. DOI.
- Vanhoefer, O.: 1996, Master Thesis, University of Kiel.
- Wang, Y., Shen, C., Liu, R., Liu, J., Guo, J., Li, X., Xu, M., Hu, Q., Zhang, T.: 2018, Understanding the twist distribution inside magnetic flux ropes by anatomizing an interplanetary magnetic cloud. *J. Geophys. Res.* **123**(5), 3238. DOI.
- Wibberenz, G., Le Roux, J., Potgieter, M., Bieber, J.: 1998, Transient effects and disturbed conditions. *Space Sci. Rev.* **83**(1–2), 309. DOI.
- Winslow, R.M., Schwadron, N.A., Lugaz, N., Guo, J., Joyce, C.J., Jordan, A.P., Wilson, J.K., Spence, H.E., Lawrence, D.J., Wimmer-Schweingruber, R.F., et al.: 2018, Opening a window on ICME-driven GCR modulation in the inner solar system. *Astrophys. J.* **856**(2), 139. DOI.
- Witasse, O., Sánchez-Cano, B., Mays, M., Kajdič, P., Opgenoorth, H., Elliott, H., Richardson, I., Zouganelis, I., Zender, J., Wimmer-Schweingruber, R., et al.: 2017, Interplanetary coronal mass ejection observed at STEREO-A, Mars, comet 67P/Churyumov–Gerasimenko, Saturn, and New Horizons en route to Pluto: comparison of its Forbush decreases at 1.4, 3.1, and 9.9 AU. *J. Geophys. Res.* **122**(8), 7865. DOI.
- Zeitlin, C., Hassler, D., Wimmer-Schweingruber, R., Ehresmann, B., Appel, J., Berger, T., Böhm, E., Böttcher, S., Brinza, D., Burmeister, S., et al.: 2016, Calibration and characterization of the Radiation Assessment Detector (RAD) on Curiosity. *Space Sci. Rev.* **201**(1–4), 201. DOI.
- Zhuang, B., Wang, Y., Shen, C., Liu, S., Wang, J., Pan, Z., Li, H., Liu, R.: 2017, The significance of the influence of the CME deflection in interplanetary space on the CME arrival at Earth. *Astrophys. J.* **845**(2), 117. DOI.